The *Chlamydia* type III effector TarP alters the dynamics and organization of host cell focal adhesions

António T. Pedrosa[b,c,1], Korinn N. Murphy[a,b], Ana T. Nogueira[b,c,2], Amanda J. Brinkworth[a], Tristan R. Thwaites[c,3], Jesse Aaron[d], Teng-Leong Chew[d], and Rey A. Carabeo[a]

[a]Department of Pathology and Microbiology, University of Nebraska Medical Center, Omaha, NE; [b]School of Molecular Biosciences, College of Veterinary Medicine, Washington State University, Pullman, WA; [c]Bacteriology Section, Programme in Microbiology, Institute of Medical Sciences, University of Aberdeen, Aberdeen, UK; [d]Advanced Imaging Center, Janelia Research Campus, Howard Hughes Medical Institute, Ashburn, VA

Corresponding author:
Rey A. Carabeo, Ph.D.
Department of Pathology and Microbiology
University of Nebraska Medical Center
Omaha, NE 68198-5900
(402) 836-9778
Email: rey.carabeo@unmc.edu

Current address:
[1]Molecular Cell Biology Laboratory, NHLBI, NIH, Bethesda, MD
[2]Department of Pharmacology, University of North Carolina at Chapel Hill, Chapel Hill, NC
[3]Cell and Gene Therapy Catapult, London, UK

Keywords: *Chlamydia*, Focal adhesion, Pathogenesis, Cell adhesion, iPALM

Abstract

The human pathogen *Chlamydia trachomatis* targets epithelial cells lining the genital mucosa. We observed that infection of various cell types, including fibroblasts and epithelial cells resulted in the formation of unusually stable focal adhesions that resisted disassembly induced by the myosin II inhibitor, blebbistatin. Super-resolution microscopy revealed in infected cells the vertical displacement of paxillin and FAK from the signaling layer of focal adhesions; while vinculin remained in its normal position within the force transduction layer. The candidate type III effector TarP which localized to focal adhesions during infection and when expressed ectopically, was sufficient to mimic both the reorganization and blebbistatin-resistant phenotypes. These effects of TarP, including its localization to focal adhesions required interaction with the host protein vinculin through a specific domain at the C-terminus of TarP. The consequence of *Chlamydia*-stabilized focal adhesions was restricted cell motility and enhanced attachment to the extracellular matrix. Thus, via a novel mechanism, *Chlamydia* inserts TarP within focal adhesions to alter their organization and dynamics.

44 **Introduction**

45 Bacterial infection of mucosal epithelial cells triggers the antimicrobial defense strategy of cell
46 exfoliation and apoptosis induction (reviewed in: Kim *et al.*, 2010). The controlled extrusion of
47 damaged host cells and colonizing pathogens requires the degradation of cell adhesion factors.
48 In epithelial cells, focal adhesions and hemidesmosomes are primarily responsible for
49 attachment to the extracellular matrix, and their assembly and turnover are exquisitely regulated
50 at multiple levels, by kinases, phosphatases, protein-protein interactions, internalization of
51 components, and degradation (Borradori and Sonnenberg, 1999; Geiger *et al.*, 2001; Rosenblatt
52 *et al.*, 2001; Zaidel-Bar *et al.*, 2007). Disruption of one or more of these regulatory processes
53 alters the adhesion dynamics and properties of the cells.

54 One strategy employed by bacteria to neutralize exfoliation relies on the precise
55 targeting of one or more components of the focal adhesion proteome. The best-characterized
56 example is that of *Shigella*, which neutralizes epithelial extrusion to colonize the epithelium
57 efficiently (Kim *et al.*, 2009). It does so by delivering the OspE effector by the type III secretion
58 system (T3SS). This protein reinforces host cell adherence to the basement membrane by
59 interacting with integrin-linked kinase (ILK), a serine/threonine kinase that is part of the focal
60 adhesome (Kim *et al*., 2009; Zaidel-Bar *et al*., 2007). A consequence of the OspE-ILK
61 interaction is an increased surface expression of β1-integrin, which in turn promotes focal
62 adhesion (FA) assembly. In addition, the OspE-ILK complex stabilizes the focal adhesions (FAs)
63 by reducing phosphorylation of focal adhesion kinase (FAK) at a functionally important Tyr397
64 residue and of paxillin. Inhibition of both phosphorylation events has been shown to induce FA
65 disassembly (Kim *et al.*, 2009). Interestingly, some EPEC and EHEC strains, as well as
66 *Citrobacter rodentium* possess the effector EspO, which shares strong homology with OspE
67 (reviewed in Vossenkämper, Macdonald and Marchès, 2011; Morita-Ishihara *et al.*, 2013). As
68 such, it is conceivable that these pathogens also reinforce adherence of the infected epithelial
69 cells to secure an infectious foothold. The EspZ effector of EPEC and EHEC has been shown to
70 reduce cell death and detachment *in vitro* (Shames *et al.*, 2010). EspZ binds the
71 transmembrane glycoprotein CD98 and enhances its effect on β1-integrin signalling and cell
72 survival via activation of FAK (Shames *et al.*, 2010).It is possible that EspO and EspZ may
73 cooperate to confer enhanced adhesion of the host epithelial cells to the extracellular matrix.
74 Finally, through interaction with human carcino-embryonic antigen-related cell adhesion
75 molecules (CEACAM), bacterial pathogens such as *Neisseria gonorrhoeae*, *Neisseria*
76 *meningitidis*, *Moraxella catarrhalis*, and *Haemophilus influenzae* can activate β1-integrin
77 signalling and inhibit epithelial cell detachment (reviewed in: Kim *et al.*, 2010). Despite

78 numerous examples of pathogens manipulating host cell adhesion, the details of these
79 mechanisms remain uncharacterized.
80 Chlamydiae are obligate intracellular pathogens that are distinguished by their biphasic
81 developmental cycle that alters between the infectious elementary body (EB), and the
82 replicative, but non-infectious reticulate body (RB). At late time points, the non-infectious RBs
83 convert back to EBs to produce infectious particles for the next round of infection. The entire
84 intracellular growth cycle of *Chlamydia* takes ~48–96 h and occurs within a membrane-bound
85 inclusion, and most of it is spent in the non-infectious RB form. Thus, it is essential that the
86 adhesion of the infected cells to the epithelium is sustained during chlamydial development to
87 enable the differentiation of the non-infectious RBs to the infectious and stable elementary
88 bodies (EBs) (reviewed in AbdelRahman and Belland, 2005). This means that *Chlamydia* must
89 evade a host of anti-microbial defenses, including epithelial extrusion.
90 Previous works by Kumar and Valdivia (2008) and Heymann *et al.*, (2013) described the
91 loss of motility of *Chlamydia*-infected epithelial cells. Heymann *et al.*, (2013) attributed this to the
92 chlamydial inhibition of Golgi polarization that occurs at >24 h post-infection, leading to loss of
93 directional migration. In this report, we offer an alternate and possibly complementary
94 mechanism of FA stabilization, which could lead to an increase of host-cell adhesion to the
95 extracellular matrix (ECM), thus culminating in previously reported loss of motility (Kumar and
96 Valdivia, 2008; Heymann *et al.*, 2013). Using quantitative confocal and live-cell imaging and
97 super-resolution microscopy, we describe the various *Chlamydia* infection-dependent changes
98 that occur to FAs, such as increased numbers, enhanced stability, and altered organization. We
99 provide evidence implicating the T3SS effector TarP, and its interaction with the focal adhesion
100 protein vinculin. We show that vinculin and its binding motif in TarP is required for the
101 localization of the effector to focal adhesions, and their resistance to blebbistatin-induced
102 disassembly. TarP localization to focal adhesions is also required for the displacement of the
103 focal adhesion kinase and paxillin from their normal position within the integrin signaling layer.
104 We also show that TarP alone was sufficient to restrict cell motility. Overall, the results indicate
105 that *Chlamydia* has a dedicated mechanism of modulating focal adhesion dynamics, which may
106 be linked to the maintenance of *Chlamydia* infection in a high-turnover tissue site.
107
108 **RESULTS**
109 ***Chlamydia infection enhances FA numbers***
110 Cos7 cells were infected and 24 h post-infection (hpi), cells were fixed and prepared for indirect
111 immunofluorescence imaging of paxillin-positive FAs. As shown in **Figure 1**, cells infected with

112 *C. trachomatis* serovar L2, serovar D, serovar B, *C. caviae* GPIC, and *C. muridarum* (MoPn)
113 consistently had greater numbers of FAs than mock-infected cells. We further explored the
114 apparent infection-dependent increase in FA numbers using serovar L2, and observed
115 enhanced FA numbers at 8 hpi that increased by 24 hpi. Next, we asked if the process is
116 pathogen-directed. Specifically, we investigated if this effect on FAs required de novo protein
117 synthesis by *Chlamydia*. Cos7 cells were infected with CtrL2 for the specified duration followed
118 by treatment by the bacterial translation inhibitor, chloramphenicol (Cm). We observed that
119 while an 8-h protein synthesis inhibition was not sufficient to prevent the effects on FA number,
120 the 24-h Cm treatment reduced FA numbers of infected cells to the level of mock-infected
121 control (**Figure 2**). The results indicate that the latter phase of focal adhesion alterations
122 requires either the *de novo* synthesis of new proteins by *Chlamydia* or replenishment of
123 effectors packaged in the metabolically quiescent EBs. These effectors are delivered by the
124 type III secretion system early in infection, prior to differentiation to the vegetative reticulate
125 body form, when they gain the ability for macromolecular synthesis.
126 A marked difference was the increased numbers of FAs at the interior relative to the cell
127 periphery. Focal adhesion maturation is associated with movement away from the cell periphery
128 and towards the center (Smilenov, et al. 1999). FAs at the interior of the cell either mature to
129 become stable fibrillar adhesions to promote cell attachment or disassemble during migration
130 (Smilenov, et al. 1999 ; Dumbauld *et al.*, 2010; reviewed in: Nagano *et al.*, 2012). We speculated
131 that the increased numbers of interior FAs arose from infection-dependent stabilization. To
132 assess stability, we took advantage of the enhanced turnover of FAs in the presence of the
133 myosin II-specific inhibitor, blebbistatin (Straight *et al.*, 2003). FA stability is dependent on
134 tension within and between focal adhesions (Chrzanowska-Wodnicka and Burridge, 1996;
135 Pasapera *et al.*, 2010; Carisey *et al.*, 2013). This tension is largely provided by the contractile
136 action of the molecular motor myosin II on stress fibers (SF); and its inhibition by blebbistatin
137 consistently leads to FA disassembly and altered motility (Wang *et al.*, 2008; Dumbauld *et al.*,
138 2010, Liu *et al.*, 2010). We evaluated the relative resistance of FAs to a 60-min treatment with
139 10 μM blebbistatin in the context of infection with CtrL2 at 20 hpi. As shown in **Figure 3** of
140 representative samples, SFs in the mock-infected cell disassembled, with the simultaneous
141 disappearance of FAs marked with paxillin. In contrast, FAs in the CtrL2-infected cells
142 remained. Infection did not prevent blebbistatin-induced disassembly of stress fibers. Taken
143 together, the results point to a dedicated mechanism in *Chlamydia trachomatis* and perhaps
144 other chlamydial species to stabilize focal adhesions. In addition, focal adhesion stabilization in
145 infected cells did not require stress fibers.

146

147 ***The type III effector TarP localizes to focal adhesions in a vinculin-dependent manner***

148 The chlamydial type III effector TarP has been implicated in the invasion process during
149 infection of non-phagocytic cells. Specifically, TarP translocation by the elementary bodies
150 contributes to the actin remodeling that is required for uptake of the pathogen (Clifton *et al.*,
151 2005; Jewett *et al.*, 2006; Lane *et al.*, 2008; Thwaites *et al.*, 2014). Interestingly, TarP was also
152 reported to have a role in increased resistance of infected cells to apoptosis, raising the
153 possibility that this effector has post-invasion function (Mehlitz *et al.*, 2010). Consistent with this
154 idea is the continuous presence of the protein throughout infection (Clifton *et al.*, 2004). In
155 addition, there was sustained presence of TarP translocated to the cytosol as indicated by its
156 reactivity to the anti-phosphotyrosine 4G10 antibody under conditions that prevented further
157 synthesis of this protein, i.e. Cm treatment (**Figure S1**). During invasion, TarP localizes to sites
158 of chlamydial adhesion at the plasma membrane (Clifton *et al.*, 2004). If TarP has a role post-
159 invasion, we expect TarP to be found at sites where it exerts its function. Immunostaining with a
160 rabbit polyclonal antibody to C. *trachomatis* serovar L2 (CtrL2) TarP of infected mouse
161 embryonic fibroblasts (MEFs) revealed specific staining of focal adhesions (FA), in addition to
162 punctae within inclusions, which are likely to be the bacteria (**Figure 4**). Uninfected cells
163 consistently exhibited diffused background immunofluorescence signal, illustrating specificity of
164 the antibody to TarP localized to FAs.

165 We then sought to determine if ectopically expressed TarP would yield a similar
166 subcellular localization to FAs. TarP and its deletion derivatives shown in Figure 5A were fused
167 to the fluorescent protein mTurquoise2, and ectopically expressed in MEFs . TarP has multiple
168 domains that resemble motifs for protein-protein interaction and signaling, including a repeated
169 50-amino acid domains that is tyrosine-phosphorylated by Src family kinases and the Abl
170 kinase, actin-binding domains, a leucine-aspartate (LD) domain recognized by the focal
171 adhesion kinase (FAK), and vinculin-binding domains (VBD) (Clifton *et al*., 2005; Jewett *et al*.,
172 2006, 2010; Lutter *et al*. 2010; Mehlitz *et al*. 2010; Jiwani *et al*., 2013; Thwaites *et al*., 2014,
173 2015; Braun *et al*., 2019*)* . All have been demonstrated in invasion-related actin-recruitment
174 assays to be functional(Lane *et al*., 2008; Thwaites *et al*., 2014, 2015) . We created various C-
175 terminal deletion constructs of TarP fused to mTurquoise for heterologous expression in MEFs,
176 as well as a TarP derivative lacking the proline-rich domain (PRD) to minimize non-specific
177 aggregation of the protein. Transfected cells were counterstained with a monoclonal antibody to
178 paxillin to visualize FAs. As shown in **Figure 5B**, colocalization of TarP with the focal adhesion

179 marker paxillin required the LD and VBD motifs. Note that paxillin localization was observed for
180 both full-length TarP and TarP ΔPRD (**Figure S2**)
181 We previously reported that the LD and VBD domains were recognized by FAK and
182 vinculin, respectively (Thwaites *et al*., 2014, 2015). They are distinct non-overlapping domains
183 that interacted with their respective binding partners independently. Therefore, we evaluated if
184 the loss of either of the binding partner (e.g. FAK or vinculin) would result in the loss of FA
185 localization. To address the functional relevance of these interactions, albeit in a post-invasion
186 context, the LDVBD construct was expressed in wild type, *vcl*-/- (vinculin), or *ptk2*-/- (FAK) MEF
187 knockout mutants. We observed FA localization of mTurquoise-LDVBD in wild type MEFs, but
188 not in *vcl*-/- MEFs (**Figure 5B**). The loss of FAK did not affect the focal adhesion localization of
189 LDVBD (**Figure 5C**). Together the data indicated that TarP localization to FAs required the host
190 protein vinculin, likely through its interaction with the VBD domain. FAK was dispensable in this
191 regard. The TarP-positive subcellular structures were verified as FAs based on β1-integrin
192 staining using a monoclonal antibody specific to the conformationally active form of the receptor
193 (**Figure 5D**).
194
195 ***The ectopic expression of TarP is sufficient to increase focal adhesion numbers and***
196 ***confer vinculin-dependent resistance to blebbistatin***
197 We observed increased paxillin-positive FAs in TarP-transfected cells, provided that the TarP
198 construct retained the VBD domain. Images from the FA localization experiments in Cos7 cells
199 were re-analyzed by quantifying the number of focal adhesions per cell in cells transfected with
200 the mTurquoise vector alone, full-length TarP, or LDVBD (**Figure 6A**). Paxillin-positive
201 structures in transfected cells were counted in NIH ImageJ, and the data is illustrated as box-
202 whisker plots in **Figure 6B**. We observed statistically significant increases in focal adhesion
203 numbers in cells expressing TarP ΔPRD and LDVBD. These results suggested that the ability of
204 TarP to localize to FAs, which was mediated by the LDVBD domain of TarP was linked to its
205 effects on FA numbers.
206 We also evaluated the effect of ectopically expressed LDVBD on the stability of focal
207 adhesions in fixed cells. As illustrated in **Figure 7A**, *Chlamydia*-infected wild type MEFs
208 retained paxillin-marked FAs after 60 min of treatment with 10 uM blebbistatin, while mock-
209 infected cells lost them. In contrast, infection of the *vcl*-/- MEFs failed to inhibit blebbistatin-
210 induced disassembly of focal adhesions, highlighting the crucial role of the host protein vinculin
211 in FA stability. Using these results as reference, we investigated if the LDVBD domain was
212 sufficient to confer a similar level of resistance to blebbistatin-induced disassembly, and if it did

213 so in a vinculin-dependent manner. LDVBD transfection of wild type MEFs led to the retention of
214 FAs after the 60-min treatment with blebbistatin, while the *vcl*-/- MEFs lost these structures
215 despite LDVBD expression (Figure 7B). Therefore, we concluded that vinculin plays an
216 important role in TarP-dependent stabilization of FAs. However, we could not determine if the
217 apparent stabilizing role of vinculin is due to the FA localization of TarP or an alteration of its
218 activity as a result of its interaction with TarP.
219
220 ***Infection disrupts the stratified organization of focal adhesions, a phenotype mimicked***
221 ***by the ectopic expression of TarP***
222 Focal adhesions are organized into distinct strata termed the integrin layer, the signaling layer,
223 which harbors paxillin and FAK amongst others, and the force transduction layer that contains
224 vinculin, talin, and other mechanosensitive proteins. At the highest layer, actin and actin-
225 associated proteins, such as α-actinin and myosin II are found (Betzig *et al.*, 2006;
226 Kanchanawong *et al.*, 2010). Given the profound effect of infection and TarP ectopic expression
227 on FA stability, we investigated using interferometric photoactivated localization microscopy
228 (iPALM) their effects on FA organization. The localization of paxillin, FAK, and vinculin, all fused
229 to mTurquoise2 were monitored in mock-infected, CtrL2-infected, TarP full-length, or LDVBD-
230 transfected cells (**Figure 8**). Image analysis revealed dramatic reorganization of FAs with
231 regards to paxillin and FAK. In control samples, paxillin, FAK, and vinculin were found 50.5,
232 40.4, and 71 nm from the bottom of the cell, respectively, consistent with previous findings
233 (Kanchanawong *et al.*, 2010). However, paxillin and FAK shifted upwards to 176.9 and 96 nm,
234 respectively in infected cells, while no change in location was observed for vinculin (**Figure 8A**).
235 The state of infection of cells analyzed are shown in **Figure S3**.
236 Expression of TarP ΔPRD also caused a shift (240.2 nm) in paxillin localization (**Figure**
237 **8B**). LDVBD expression caused a noticeable shift (47 nm, with a second peak at 130 nm), but to
238 a lesser degree than full-length TarP. Interestingly, vinculin was not affected by either infection
239 or TarP ΔPRD (or LDVBD) expression, which points to the specific disruption of FA organization
240 by *Chlamydia*.
241
242 ***Cell motility is restricted in Chlamydia-infected or TarP-expressing cells***
243 It was previously reported that *Chlamydia*-infected cells were restricted in their motility, and this
244 was attributed to the inability of infected cells to establish front-rear polarity due to Golgi
245 fragmentation induced by the pathogen. We decided to reinvestigate the loss of motility of
246 infected cells by focusing on focal adhesion dynamics. The decision of the cell to migrate or

247 adhere involves the regulation of focal adhesion stability in response to external cues, such as
248 chemoattractants and extracellular matrix (ECM) stiffness. First, we verified that *Chlamydia*-
249 infected mouse embryo fibroblasts were severely limited in their ability to migrate, relative to
250 mock-infected control cells (Movie S1). The manual tracking plugin of ImageJ was utilized to
251 obtain cell trajectory tracks for the motility assay. Cells were tracked using the position of the
252 nucleus over time. The coordinate data was input into ibidi's chemotaxis and migration tool to
253 obtain velocity and distance measurements. Velocity measurements revealed a 1.5-fold
254 decrease in the mean rate of migration of infected cells (**Figure 9A and 9C**).
255 Mouse embryonic fibroblasts were transfected to ectopically express mTurquoise2
256 vector only or the LDVBD domain. Cell migration was monitored in the DIC channel with
257 fluorescence images taken at the end of the motility assay (**Movie S1**; **Figure S4**). To quantify
258 motility, the cells were tracked as described above, with accompanying velocity calculations. As
259 shown in **Figure 9A and 9B**, transfected cells were significantly restricted in their motility
260 relative to mock-transfected controls. Both distance and velocity of LDVBD-transfected cells
261 were further restricted to those of infected cells (**Figure 9C**) indicating that inhibition of cell
262 migration by *C. trachomatis* could be accounted for fully by TarP overexpression. The enhanced
263 inhibition of migration distance and velocity in transfected cells may have been due to increased
264 levels of LDVBD when compared to levels present during infection.
265
266 ***Infection by Chlamydia trachomatis but not ectopic expression of TarP confers***
267 ***resistance to detachment by mild trypsinization***
268 Exfoliation of epithelial cells from the infected epithelium has been reported in rodent models of
269 ocular and genital infection; and both reports speculated the involvement of neutrophil-derived
270 proteases in the process (Ramsey *et al.*, 2005; Lacy *et al.*, 2011). We evaluated the resistance
271 of infected epithelial cells to detachment by 0.025% trypsin, and monitored for cell rounding by
272 time-lapse imaging at 1-min intervals for 30 min (Movie 1). Uninfected HeLa cells started
273 detaching by 7 min post-trypsinization, while *C. trachomatis* L2-infected cells remained attached
274 through the duration of imaging (30 min C. *trachomatis* post-trypsinization). To evaluate if TarP
275 ectopic expression would be sufficient to resist detachment, the cells were transfected for 24 h
276 to overexpress (LDVBD-mTurquoise2). Monolayers were imaged under fluorescence
277 microscopy at 0, 15, and 30-min after trypsinization. If TarP LDVBD overexpression was
278 sufficient to induce detachment resistance, we would expect an enrichment in remaining
279 adherent cells of those expressing LDVBD-mTurquoise2 than cells expressing mTurquoise2
280 only. Percentage values for both LDVBD-mTurquoise2 and vector-only samples were 11.9%

281 vs. 11.0% prior to trypsinization. We obtained the following for LDVBD vs. vector-only; 10.2%
282 vs. 10.3% (15 min) and 8.7% vs. 11.0% (30 min). No statistically significant differences were
283 found between LDVBD and vector only for either trypsinization time point. These results
284 indicated that, while TarP is able to reduce cell motility, it was not sufficient to confer resistance
285 to detachment by mild trypsinization. We interpret this to mean that additional changes to focal
286 adhesions, possibly mediated by additional chlamydial factors are required.
287
288

289 **Discussion**

290 All chlamydial species, to varying extents exhibit tropism to epithelial cells, and thus likely
291 evolved to counteract cell extrusion associated with the normal cycle of turnover of the
292 epithelium, or as an anti-microbial mechanism to limit dissemination and eliminate infection. The
293 latter may also involve polymorphonuclear (PMN) cells, which secrete proteases to degrade
294 adhesion structures of epithelial cells. Thus, *Chlamydia*, with its biphasic developmental cycle
295 that involves a temporary loss of infectivity, is subjected to a very strong selective pressure to
296 acquire mechanisms to inhibit epithelial cell extrusion. A large portion of the developmental
297 cycle is spent in the non-infectious form, and thus, it is crucial to the survival of the pathogen to
298 inhibit extrusion of host epithelial cells before *Chlamydia* could convert to the infectious form.
299 Here, we demonstrated that adhesion of infected cells is enhanced via the action of TarP, an
300 effector protein conserved in the genus *Chlamydia*, and the host cell protein vinculin.

301 Our data collectively point to FAs as targets for modulation by *Chlamydia*. The type III
302 effector TarP plays a role in this modulation. The mechanism involves the vinculin-dependent
303 localization of TarP to FAs resulting in increased stability as indicated by their resistance to
304 disassembly by the myosin II inhibitor blebbistatin. We also made the novel observation of FA
305 reorganization in *Chlamydia*-infected or TarP-expressing cells, with paxillin and FAK displaced
306 from the signaling layer. A pressing question is whether the reorganization is the cause or the
307 effect of enhanced stability of TarP-targeted FAs. Considering the reported relative stability of
308 FAs in FAK-depleted cells, it is possible that the displacement of FAK by TarP could be
309 analogous to a loss-of-function. A more comprehensive investigation of FA disorganization by
310 TarP is required to define the exact mechanism of FA stabilization by this chlamydial effector.
311 We did not observe any change to tyrosine autophosphorylation at position 397; and we cannot
312 exclude the possibility that despite the apparent phosphorylation level, FAK displacement might
313 negatively affect interactions with signaling proteins that recognize and bind this motif, like the
314 Src kinase. The progression of tyrosine phosphorylation along the FAK protein by Src is crucial
315 to the role of FAK in disassembling FAs. Therefore, restricted FAK-Src interaction as a
316 consequence of FAK displacement in infected cells remains a possibility. Paxillin was similarly
317 displaced in both infected and TarP-expressing cells, which likely disrupts protein-protein
318 interactions and signaling related to paxillin within FAs. To our knowledge, FA reorganization to
319 the extent that we observed in infected cells has not been reported, pointing to a possible novel
320 mechanism of regulating FA dynamics.

321 While TarP, specifically the LDVBD domain was sufficient to drive FA stability to inhibit
322 cell motility, it was unable to mimic the resistance of infected cells to detachment by mild

323 trypsinization, which was meant to replicate polymorphonuclear cell (PMN)-mediated extrusion
324 of infected epithelial cells. This would be consistent with the involvement of additional
325 chlamydial factors that may mediate various aspects of focal adhesion characteristics, in
326 addition to numbers. Additional factors may facilitate progression of maturation, possibly to
327 fibrillar adhesions. Another might be the infection-dependent production of extracellular matrix
328 components by the host cell, including collagen. Increased deposition of collagen underneath
329 infected cells would likely influence FA stability by engaging integrins and inducing "outside-in"
330 FA-stabilizing signals. Thus, *Chlamydia* might have multiple cooperating mechanisms ensuring
331 the strong adhesion of its host cell, highlighting the importance of a mechanism to counteract
332 epithelial cell extrusion.
333 A pressing question is the biological significance of FA stabilization by this pathogen. We
334 speculate that this might be one mechanism by which *Chlamydia* neutralize extrusion of
335 epithelial cells. It is known that this process could limit infection dissemination. Shedding of
336 epithelial cells from uropathogenic *E. coli* (UPEC)-infected bladder is thought to reduce bacterial
337 burden, facilitating resolution of infection (Mysorekar *et al.*, 2002). The intestinal pathogen
338 *Shigella* possesses an effector, OspE that modulates epithelial cell attachment to facilitate the
339 pathogen's cell-to-cell spread. Indeed, loss of OspE resulted in a significant decrease in
340 virulence (Kim *et al.*, 2009, 2010). Epithelial cells of the genital tract or the ocular mucosa also
341 experience higher rates of turnover and are constantly replenished (Kuwabara, Perkins and
342 Cogan, 1976; Crosson, Klyce and Beuerman, 1986; Anderson, Marathe and Pudney, 2014).
343 Epithelial extrusion is a complex process that involves, not only promoting detachment of the
344 cells from the ECM, but also modulating interactions with neighboring cells via disassembly of
345 intercellular junctions (Rosenblatt, Raff and Cramer, 2001; Gudipaty and Rosenblatt, 2017).
346 Another possibility is increased resistance to apoptosis. Cell detachment is associated with
347 anoikis, a programmed cell death associated with loss of adherence (Frisch and Francis, 1994;
348 Gudipaty *et al.*, 2018). Focal adhesions provide anti-apoptotic signals (Frisch *et al.*, 1996), and
349 *Chlamydia* stabilization of these structures could promote apoptosis resistance.
350 An interesting question is the means by which epithelial cell extrusion is triggered. Is it
351 part of the normal cell turnover during tissue remodeling/renewal, or is it linked to pathogen
352 recognition? The shedding of bladder epithelial cells during UPEC infection requires the
353 expression of bacterial Type 1 pili, which is a potent pathogen-associated molecular pattern
354 (PAMP) that is recognized by the toll-like receptor 4 (TLR4) (Mysorekar *et al.*, 2002), raising the
355 intriguing possibility of a direct link between regulation of cell adhesion dynamics and pathogen
356 recognition. Various chlamydial species are recognized by toll-like receptors expressed on

357 epithelial cells e.g. TLR2, TLR3, TLR4, and TLR9 (Derbigny, Kerr and Johnson, 2005;
358 O'Connell *et al.*, 2006; Shaw *et al.*, 2011; Derbigny *et al.*, 2012; Pan *et al.*, 2017; Carrasco *et*
359 *al.*, 2018; Kumar *et al.*, 2019), which may be indicative of epithelial detachment being linked to
360 pathogen recognition.
361 In addition to the demonstration that all tested *Chlamydia* species exhibited enhanced
362 FA stability, the presence of a type III effector with FA modulating function highlights the
363 importance of this process to *Chlamydia*; and yet, this aspect of Chlamydia-host cell interaction
364 is relatively understudied. The availability of a *Chlamydia* mutant lacking TarP and an efficient
365 method to image epithelial cell extrusion in the genital tract of animal models of infection are
366 critical to advancing studies in this area.
367
368
369

370 **Materials and Methods**

371 **Cell culture.** Cos7 (ATCC CRL-1651), NIH3T3 (kindly supplied by Hector Aguilar-Carreño
372 ATCC CRL-1658) and HeLa 229 (ATCC CCL-2.1) Mouse embryonic fibroblasts (MEFs) *vcl*$^{-/-}$
373 and matched HeLa 229 MEFs *vcl*$^{+/+}$ (Marg *et al.*, 2010) (were kindly provided by Dr. Wolfgang
374 Ziegler Hannover Medial School).cells were culture using Dulbecco's Modified Eagle Medium
375 (DMEM) (Thermofisher scientific, 11960-085). Media were supplemented with 10% fetal bovine
376 serum (Sigma, F0804-500ML), 2mM L-glutamine, and 10µg/ml gentamicin. The human
377 keratinocytes HaCaT cells (kindly supplied by Dr. Kristin M. Braun) were cultured in 3 parts
378 DMEM and 1 part Ham's F-12 Nutrient Mix (Thermofisher scientific 11765054), supplemented
379 with 10% fetal bovine serum (Sigma, F0804-500ML), 2 mM L-glutamine, 10µg/ml gentamicin,
380 insulin (Sigma I9278-5ML) and hydrocortisone cholera toxin EGF (HCE) cocktail. *Chlamydia*
381 *trachomatis* serovar L2 (L2/434/Bu) was propagated in HeLa 229. EBs were harvested by
382 discontinuous density gradient centrifugation in gastrografin (Bracco Diagnostics), as previously
383 described (Thwaites *et al.*, 2014).
384

385 ***Chlamydia* infections.** Cells were infected with *Chlamydia trachomatis* serovar L2 (L2/434/Bu,
386 CtrL2) at the multiplicity of infection MOI of 5, for 20 h, and of 25, for 8 h, in ice cold serum-free
387 DMEM. Cells were centrifuged at 1000 rpm for 5 min at 4 °C to synchronize the infection. After
388 centrifugation, the inoculum was replaced with warm DMEM supplemented with 10% fetal
389 bovine serum, 2 mM L-glutamine, and 10µg/ml gentamicin. In parallel, a mock-infected control
390 was made following the same protocol but without *Chlamydia* infectious particles. Infection by
391 other strains/serovars was as follows. Cos7 cells were grown on glass coverslips. Cells were
392 infected with *Chlamydia trachomatis* serovar L2, serovar D, serovar B, *Chlamydia muridarum*
393 (MoPn), or *Chlamydia caviae* (GPIC) at an MOI of 5 for 24 hours. Cells were centrifuged at 500
394 x g for 15 minutes at 4°C to synchronize the infection. A mock-infected control was made
395 following the same protocol but without *Chlamydia* infectious particles. Prior to infection with
396 Serovar D, cells were pre-treated with 1x DEAE-Dextran for 15 minutes at room temperature.
397 Pre-treatment was followed by two washes with 1x HBSS and replacement with DMEM to
398 continue the infection.
399

400 **Immunostaining.** Cells were grown on fibronectin coated coverslips (Neuvitro, GG-12-
401 fibronectin) for the duration of the experiment. At the pre-determined, time cells were rinsed with
402 Hank's Balanced Salt Solution (HBSS) (Thermofisher scientific, 14025-100) and fixed using 4%
403 paraformaldehyde (PFA) in PBS pH 7.4 (Gibco, 14190-094) for 20 min at room temperature.

404 The fixed cells were then permeabilized using PBS with 0.2% Triton X-100. Subsequently,
405 permeabilized cells were incubated with 1% BSA (Sigma, A9418) in PBS for 30 min at room
406 temperature to block non-specific antigen binding. Cells were then incubated with the primary
407 antibodies overnight at 4ºC with rocking. The primary antibodies used in this study were rabbit
408 polyclonal antibody against FAK phosphorylated at tyrosine 397 (pFAK-Y397) (Abcam, ab4803),
409 rabbit monoclonal antibody paxillin (Abcam, ab32084), mouse monoclonal antibody vinculin
410 (Abcam, ab18058), rat monoclonal 9EG7 against the active form of β1-integrin (BD Biosciences,
411 553715), mouse monoclonal Flag-tag antibody (Cell Signalling, 8146S) mouse monoclonal
412 antibody *Chlamydia* LPS (Abcam, ab62708) and convalescent human sera. Afterwards cells
413 were incubated with appropriate fluorescently conjugated secondary antibodies and, when
414 specified, with DAPI (Roche, 10236276001) and Alexa flour 488 phalloidin stains, for 1 hr at
415 room temperature, with rocking. In this study, the following secondary antibodies were used:
416 goat anti-rabbit Alexa flour 488 (Thermofisher Scientific, A11008), goat anti-rabbit Alexa flour
417 633 (Thermofisher Scientific, A21071), goat anti-mouse Alexa flour 594 (Thermofisher Scientific,
418 A11005), goat anti-human Alexa flour 647 (Thermofisher scientific A-21445). Following staining,
419 the coverslips were mounted with Mowiol, and visualized in ZEISS LSM 710 confocal
420 microscope, in the Microscopy and Histology Core Facility at the University of Aberdeen, or the
421 Leica SP8 confocal microscope in Washington State University Integrative Physiology and
422 Neuroscience advance image equipment. FIJI software (Schindelin *et al.*, 2012; Schneider,
423 Rasband and Eliceiri, 2012) was used to generate the final images.
424 To localize endogenous TarP to focal adhesions, Mouse embryonic fibroblasts (MEFs)
425 grown on glass coverslips were infected with *Chlamydia trachomatis* L2 at an MOI of 10 for 20
426 hours. Cells were centrifuged at 500G for 15 minutes at 4°C to synchronize the infection. A
427 mock-infected control was made following the same protocol but without *Chlamydia* infectious
428 particles. Cells were fixed using ice cold 100% methanol for one minute. Cells were then
429 blocked with 5% BSA for one hour at room temperature. Focal adhesions and TarP were
430 visualized respectively using a primary monoclonal Talin1 antibody (Novus Biologics, NBP2-
431 50320) and rabbit polyclonal TarP antibody generated against the epitope (661-710 a.a.) (Li
432 International, Denver, CO). Samples were incubated overnight at 4°C. Immunostaining with
433 secondary antibodies was as described above.
434
435 **Time-lapse microscopy.** For live-cell imaging of FAs fibroblasts were seeded on ibidi μ-slide 8
436 well chambers with fibronectin coating (ibidi, 80823) at the recommended seeding density and
437 left overnight in a 37 ºC, 5% CO_2 incubator. The following day, cells were infected with CtrL2

438 with a MOI of 5. At 2 h post-infection, the cells were transfected with either Vinculin-venus
439 (Grashoff *et al.*, 2010) a gift from Martin Schwartz, (Addgene, 27300), paxillin-pEGFP (Laukaitis
440 *et al.*, 2001) a gift from Rick Horwitz, (Addgene, 15233), or FAK-GFP (Gu *et al.*, 1999; Lane *et*
441 *al.*, 2008) a gift from Kenneth Yamada, (Addgene, 50515) using Lipofectamine 3000
442 transfection reagent (Thermofisher Scientific, L3000008), following the manufacture instructions.
443 After 20 to 22 h, time lapsed images of transfected cells were obtained using a Leica SD6000
444 AF in TIRF mode, in Washington State University IPN advance image equipment. Images of the
445 GFP-tagged proteins were collected every minute for 90 min. The time lapse images were
446 uploaded to the Focal adhesion Analysis server (Berginski and Gomez, 2013).
447
448 **Cell Motility Assay.** Mouse embryonic fibroblasts (MEFs) were seeded on ibidi μ-slide live cell
449 imaging chambers (ibidi, 80426). Cells were infected with *Chlamydia trachomatis* serovar L2 at
450 an MOI of 10 by rocking at 4°C for one hour. Infected cells were imaged starting at 20 hours
451 post-infection. A mock-infected control was made following the same protocol but without
452 *Chlamydia* infectious particles. Cells were transfected with N1-mTurquoise2 empty vector
453 control or TarP$^{829-1006}$-mTurquoise2 (LDVBD) using electroporation, seeded into an ibidi μ-slide,
454 and imaged starting at 22 hours post electroporation. Cells were imaged in live cell imaging
455 solution (Thermofisher scientific, A14291DJ) supplemented with 5% fetal bovine serum within a
456 37°C, 5% CO_2 controlled environment. Time-lapse DIC images were obtained using a Leica
457 SD6000 AF microscope every ten minutes for ten hours. To minimize the risk of phototoxicity,
458 we restricted image acquisition of the fluorescent mTurquoise2 channel for our transfected cells
459 to the last frame alone. We utilized a similar individual cell tracking data analysis approach as
460 described in (Pijuan *et al.*, 2019). Cell motility was tracked using the manual tracking function in
461 ImageJ. Each individual cell was tracked using the position of the nucleus over time. We
462 maximized the time of analysis for each experiment based on the number of cells that remained
463 within a trackable field of view over the imaging span. The coordinate data from the manual
464 tracking function was uploaded to ibidi's chemotaxis and migration tool. Measurements were
465 taken from spatially calibrated images with a (pixel/μm) scale contained within the meta data.
466 The x/y calibration was set to 0.800001 based on the microscope's settings contained within the
467 file's meta data. The statistics function was used to determine the velocity and euclidean
468 (straight-line) distance traveled for each cell.
469
470 ***De novo* protein inhibition.** Cos7 cells were cultured as previously described. Prior to
471 infection, cells and EB particles were treated with 60 μg/ml of chloramphenicol (Sigma C0378)

472 for 30 min. Cells and EBs were kept in chloramphenicol supplemented DMEM until fixation.
473 Cells were fixed at 8 or 20 h post-infection and were immunostained as described above.
474
475 **Western blot.** Cos7 cells were plated in 6 well plates with duplicate wells and incubated at 37°C
476 and 5% CO2, until 80% confluency. Cells were infected, as previously described, with CtrL2 for
477 0 min, 8 or 24 hrs with an MOI of 200. Proteins were harvested using ice cold RIPA buffer
478 (Millipore 20-188) supplemented with phosphatase (Sigma 4906845001) and protease inhibitors
479 (Sigma 5892970001). Cells were scraped and incubated for 30 min on ice. The lysates were
480 centrifuged at 13,000 x g for 20 min at 4°C. Supernatants were diluted in Laemmli buffer (Biorad
481 161-0747) and kept at -20°C before analysis. Samples were resolved on 10% acrylamide SDS-
482 PAGE. Proteins were transferred to a nitrocellulose membrane (Bio-rad 1620115).
483 Immunoblotting was performed by blocking membranes with 5% BSA in TBS-T overnight at 4°C
484 and incubation using antibodies against TarP (a generous gift from Dr. Raphael Valdivia, Duke
485 University) and β-tubulin HRP conjugated (Abcam ab21058). The secondary antibody used was
486 anti-mouse HRP conjugated (DAKO P0161). Immobilin chemiluminescence kit (Millipore,
487 WBKLS0500) was used to develop the blot.
488
489 **Cloning and transfection of TarP contructs.** A summary of the primers used in this study is
490 provided in Table S1. Initially TarP Full-length, TarP LDVBD, TarP LD, and TarP VBD were
491 PCR amplified from CtrL2 genomic DNA using the primers combination 1-2, 5-2, 5-6 and 4-2,
492 respectively. A *Bam*H1 (reverse primer) and *Kpn*I (forward primer) restriction sites were used for
493 fusion with the N1-mTurquoise2 plasmid. The TarP ΔPRD was obtained using the 7-8 primer
494 pair for PCR amplification from TarP Full-length-mTurquoise2 fusion plasmid. The primers were
495 created to amplify the whole TarP Full-length-mTurquoise2 except the nucleotides that
496 constitute the proline rich domain (PRD) 625-650. The resulting PCR product was recombined
497 using in-Fusion HD cloning plus CE (Clontech, 638916) to create a functional circular plasmid.
498 TarP ΔLDVBD was PCR amplified from the TarP ΔPRD-mTurquoise2 plasmid using the primers
499 pair 1-3. The same restriction enzymes were used to clone these fragments into N1-
500 mTurquoise2. Transformations using restriction enzymes recombination were made into
501 chemically competent Top10 (invitrogen) *E. coli*, and vectors sequence was verified using
502 sequencing (Eurofins) The construct pFH-TarP ΔPRD and pFH-TarP ΔLDVBD used for super-
503 resolution experiments was PCR amplified from TarP ΔPRD-mTurquoise2 using primers
504 combination 9-10 and 9-17, respectively. To use homology cloning the vector backbone 1436
505 pcDNA3-Flag-HA, kindly provided by William Sellers (Addgene 10792), was linearized by PCR

506 using the primers pair 11-12 and 11-18, creating homology overhang regions to the TarP ΔPRD
507 and TarP ΔLDVBD, respectively. TarP LDVBD was amplified from CtrL2 genomic DNA using
508 the primer pairs 13-14. To use homology cloning the vector backbone 1436 pcDNA3-Flag-HA
509 was linearized by PCR using the primer pair 15-16. Fragments and vector backbone were
510 recombined using in-Fusion HD cloning plus CE (Clontech, 638916) to create a functional
511 circular plasmid. Transformations using homology recombination were made into chemically
512 competent Stellar (Clontech) *E. coli*, and vectors sequence was verified using sequencing
513 (Eurofins). The pcDNA3-Flag-Apex-Nes was a gift from Alice Ting (Addgene, 49386). The N1-
514 mTurquoise2 (Addgene, 54843). Transfections were done as described above. For iPALM
515 experiments 1µg of DNA and 2µl of sheared salmon sperm DNA were mixed together in 15µl of
516 Opti-MEM (Thermofisher scientific, 31985062), and kept on ice for 15 min. $1x10^6$ Cos7 cells
517 were resuspended in 200µl of cold Opti-MEM, mixed with the DNA solution and kept on ice for
518 30 seconds. Cells and DNA suspension were transferred to a 4mm gap cuvette (BioRad,
519 1652088) and electroporated using BioRad Gene Pulser XCell using the following settings:
520 190V; 950uF; infinity. After electroporation 1.5ml of warm growth media was added. 400µl of cell
521 solution was added to a 6 well plate well containing 1.5ml of warm growth media and the gold
522 fiducial coverslip. Cells were incubated 37°C, 4% CO_2 for 4 h to adhere to the gold fiducial
523 coverslip. Cells were washed to remove dead cells debris and further incubated for 20 h.
524
525 **iPALM imaging and analysis.** The principle of instrumentation for iPALM imaging and analysis
526 were performed as previously described (Shtengel *et al.*, 2009; Kanchanawong *et al.*, 2010)
527 with the following modifications. After 24°C of transfection cells plated in gold fiducial coverslip
528 were fixed with 0.8% PFA and 0.1% glutaraldehyde (Sigma G7526-10ML) solution (in PBS) for
529 10 min. After fixation cells were washed 3 times with PBS and quenched using 1% NaBH4
530 (Sigma, 452882-25G) solution (in PBS) for 7 min. Cells were then washed again 3 times with
531 PBS. After washing cells were immunostained (when necessary) and/or processed for iPALM
532 imaging as previously described (Kanchanawong *et al.*, 2010). The vertical coordinates relative
533 to the golden fiducial markers are indicating by a color scale from red (0 nm) to purple (250 nm).
534
535 **Trypsin assay.** Cells were plated in 24 well plates and incubated at 37°C and 5% CO2, until
536 80-90% confluency. Afterwards, cells were infected with CtrL2 with a multiplicity of infection of 5
537 for 20 h. Cells were then treated with 0.01% trypsin diluted in serum-free DMEM media at 37°C,
538 for 0, 10, 20, 30, or 35 min. Cells were fixed with 4% PFA, carefully washed with PBS and
539 stained with DAPI to count the number of remaining cells as well as to visualize *Chlamydia*

540 inclusions. Images were taken using Nikon eclipse TE2000-U. Detachment assays were
541 performed as above, and transfection procedures were as described.
542
543

Acknowledgments

We would like to thank Drs. Martin Schwartz, Rick Horwitz, Kenneth Yamada, William Sellers, Alice Ting, and Michael Davidson for various constructs obtained through Addgene; Dr. Raphael Valdivia (Duke University Medical Center) for the generous gift of the TarP antibody; Dr. Lisa Rucks (University of Nebraska Medical Center) for the *C. trachomatis* serovar D strain; the services provided by the WSU Integrated Physiology and Neuroscience imaging facilities; and Satya Khuon (AIC Janelia) for technical help and advice. This project was supported by grants from the National Institute for Food and Agriculture (#1010265), National Institutes of Health (AI065545), and start-up funds from the WSU College of Veterinary Medicine to RAC. ATP and ATN were recipients of the Fundação para a Ciência e Tecnologia, SFRH/BD/76741/2011 and SFRH/BD/86670/2012, respectively. TRT is a Medical Research Council studentship awardee. KNM was supported by the NIH Protein Biotechnology Training Grant T32 GM008336 awarded to WSU. AJB was supported by the Infectious Diseases and Microbial Immunology Training Grant T32 AI007025 awarded to WSU. iPALM data used in this publication was produced in collaboration with the Advanced Imaging Center, a facility jointly supported by the Gordon and Betty Moore Foundation and Howard Hughes Medical Institute at the Janelia Research Campus.

Author Contributions

Conceptualization, RAC; Methodology, ATP, JA, and RAC; Software, JA; Formal Analysis, ATP; Investigation, ATP, ATN, KNM, JA, AJB, and TRT; Writing – Original Draft, ATP, and RAC; Writing – Review & Editing, RAC, KNM and AJB; Funding Acquisition RAC; Resources, JA, TLC and RAC; Supervision, TLC and RAC.

Conflict of Interest

The authors have declared that no competing or financial interests exist.

573 **References**

574 **AbdelRahman, Y. M. and Belland, R. J.** (2005) 'The chlamydial developmental cycle', *FEMS*
575 *Microbiology Reviews*, 29(5), pp. 949–959. doi: 10.1016/j.femsre.2005.03.002.

576 **Anderson, D. J., Marathe, J. and Pudney, J.** (2014) 'The Structure of the Human Vaginal
577 *Stratum Corneum* and its Role in Immune Defense', *American Journal of Reproductive*
578 *Immunology*, 71(6), pp. 618–623. doi: 10.1111/aji.12230.

579 **Berginski, M. E. and Gomez, S. M.** (2013) 'The Focal Adhesion Analysis Server: a web tool for
580 analyzing focal adhesion dynamics.', *F1000Research*, 2, p. 68. doi: 10.12688/f1000research.2-
581 68.v1.

582 **Betzig, E., Patterson, G. H., Sougrat, R., Lindwasser, O. W., Olenych, S., Bonifacino, J. S.,**
583 **Davidson, M. W., Lippincott-Schwartz, J. and Hess, H. F.** (2006) 'Imaging Intracellular
584 Fluorescent Proteins at Nanometer Resolution', *Science*, 313(5793), pp. 1642–1645. doi:
585 10.1126/science.1127344.

586 **Borradori, L. and Sonnenberg, A.** (1999) 'Structure and function of hemidesmosomes: more
587 than simple adhesion complexes.', *The Journal of investigative dermatology*, 112(4), pp. 411–8.
588 doi: 10.1046/j.1523-1747.1999.00546.x.

589 **Braun, C., Alcázar-Román, A. R., Laska, A., Mölleken, K., Fleig, U. and Hegemann, J. H.**
590 (2019) 'CPn0572, the *C. pneumoniae* ortholog of TarP, reorganizes the actin cytoskeleton via a
591 newly identified F-actin binding domain and recruitment of vinculin.', *PloS one*. Edited by D. M.
592 Ojcius, 14(1), p. e0210403. doi: 10.1371/journal.pone.0210403.

593 **Carisey, A., Tsang, R., Greiner, A. M., Nijenhuis, N., Heath, N., Nazgiewicz, A., Kemkemer,**
594 **R., Derby, B., Spatz, J. and Ballestrem, C.** (2013) 'Vinculin regulates the recruitment and
595 release of core focal adhesion proteins in a force-dependent manner.', *Current biology : CB*.
596 Elsevier, 23(4), pp. 271–81. doi: 10.1016/j.cub.2013.01.009.

597 **Carrasco, S. E., Hu, S., Imai, D. M., Kumar, R., Sandusky, G. E., Yang, X. F. and Derbigny,**
598 **W. A.** (2018) 'Toll-like receptor 3 (TLR3) promotes the resolution of *Chlamydia muridarum*

599 genital tract infection in congenic C57BL/6N mice.', *PloS one*. Public Library of Science, 13(4),
600 p. e0195165. doi: 10.1371/journal.pone.0195165.
601 **Chrzanowska-Wodnicka, M. and Burridge, K.** (1996) 'Rho-stimulated contractility drives the
602 formation of stress fibers and focal adhesions', *The Journal of Cell Biology*, 133(6), pp. 1403–
603 1415. doi: 10.1083/jcb.133.6.1403.
604 **Clifton, D. R., Fields, K. A., Grieshaber, S. S., Dooley, C. A., Fischer, E. R., Mead, D. J.,**
605 **Carabeo, R. A. and Hackstadt, T.** (2004) 'A chlamydial type III translocated protein is tyrosine-
606 phosphorylated at the site of entry and associated with recruitment of actin.', *Proceedings of the*
607 *National Academy of Sciences of the United States of America*, 101(27), pp. 10166–71. doi:
608 10.1073/pnas.0402829101.
609 **Clifton, D. R., Dooley, C. A., Grieshaber, S. S., Carabeo, R. A., Fields, K. A. and Hackstadt,**
610 **T.** (2005) 'Tyrosine Phosphorylation of the Chlamydial Effector Protein Tarp Is Species Specific
611 and Not Required for Recruitment of Actin', *Infection and Immunity*, 73(7), pp. 3860–3868. doi:
612 10.1128/IAI.73.7.3860-3868.2005.
613 **Crosson, C. E., Klyce, S. D. and Beuerman, R. W.** (1986) 'Epithelial wound closure in the
614 rabbit cornea. A biphasic process.', *Investigative ophthalmology & visual science*, 27(4), pp.
615 464–73. Available at: http://www.ncbi.nlm.nih.gov/pubmed/3957565 (Accessed: 27 November
616 2019).
617 **Derbigny, W. A., Shobe, L. R., Kamran, J. C., Toomey, K. S. and Ofner, S.** (2012)
618 'Identifying a role for Toll-like receptor 3 in the innate immune response to *Chlamydia*
619 *muridarum* infection in murine oviduct epithelial cells', *Infection and Immunity*. Edited by R. P.
620 Morrison, 80(1), pp. 245–65. doi: 10.1128/IAI.05549-11.
621 **Derbigny, W. A., Kerr, M. S. and Johnson, R. M.** (2005) 'Pattern recognition molecules
622 activated by *Chlamydia muridarum* infection of cloned murine oviduct epithelial cell lines.',
623 *Journal of immunology (Baltimore, Md. : 1950)*, 175(9), pp. 6065–75. doi:
624 10.4049/jimmunol.175.9.6065.

625 **Dumbauld, D. W., Michael, K. E., Hanks, S. K. and García, A. J.** (2010) 'Focal adhesion
626 kinase-dependent regulation of adhesive forces involves vinculin recruitment to focal
627 adhesions', *Biology of the Cell*, 102(4), pp. 203–213. doi: 10.1042/BC20090104.
628 **Frisch, S. M., Vuori, K., Ruoslahti, E. and Chan-Hui, P. Y.** (1996) 'Control of adhesion-
629 dependent cell survival by focal adhesion kinase', *The Journal of Cell Biology*, 134(3), pp. 793–
630 799. doi: 10.1083/jcb.134.3.793.
631 **Frisch, S. M. and Francis, H.** (1994) 'Disruption of epithelial cell-matrix interactions induces
632 apoptosis', *The Journal of Cell Biology*, 124(4), pp. 619–626. doi: 10.1083/jcb.124.4.619.
633 **Geiger, B., Bershadsky, A., Pankov, R. and Yamada, K. M.** (2001) 'Transmembrane crosstalk
634 between the extracellular matrix--cytoskeleton crosstalk.', *Nature reviews. Molecular cell*
635 *biology*, 2(11), pp. 793–805. doi: 10.1038/35099066.
636 **Grashoff, C., Hoffman, B. D., Brenner, M. D., Zhou, R., Parsons, M., Yang, M. T., McLean,**
637 **M. A., Sligar, S. G., Chen, C. S., Ha, T. and Schwartz, M. A.** (2010) 'Measuring mechanical
638 tension across vinculin reveals regulation of focal adhesion dynamics.', *Nature*, 466(7303), pp.
639 263–6. doi: 10.1038/nature09198.
640 **Gu, J., Tamura, M., Pankov, R., Danen, E. H., Takino, T., Matsumoto, K. and Yamada, K. M.**
641 (1999) 'Shc and FAK differentially regulate cell motility and directionality modulated by PTEN.',
642 *The Journal of cell biology*. Rockefeller University Press, 146(2), pp. 389–403. doi:
643 10.1083/jcb.146.2.389.
644 **Gudipaty, S. A., Conner, C. M., Rosenblatt, J. and Montell, D. J.** (2018) 'Unconventional
645 Ways to Live and Die: Cell Death and Survival in Development, Homeostasis, and Disease.',
646 *Annual review of cell and developmental biology*, 34(1), pp. 311–332. doi: 10.1146/annurev-
647 cellbio-100616-060748.
648 **Gudipaty, S. A. and Rosenblatt, J.** (2017) 'Epithelial cell extrusion: Pathways and
649 pathologies', *Seminars in Cell & Developmental Biology*, 67, pp. 132–140. doi:
650 10.1016/j.semcdb.2016.05.010.

651 **Heymann, J., Rejman Lipinski, A., Bauer, B., Meyer, T. F. and Heuer, D.** (2013) '*Chlamydia*
652 *trachomatis* infection prevents front-rear polarity of migrating HeLa cells', *Cellular Microbiology*,
653 15(7), pp. 1059–1069. doi: 10.1111/cmi.12114.
654 **Jewett, T. J., Fischer, E. R., Mead, D. J. and Hackstadt, T.** (2006) 'Chlamydial TARP is a
655 bacterial nucleator of actin', *Proceedings of the National Academy of Sciences*, 103(42), pp.
656 15599–15604. doi: 10.1073/pnas.0603044103.
657 **Jewett, T. J., Miller, N. J., Dooley, C. A. and Hackstadt, T.** (2010) 'The conserved Tarp actin
658 binding domain is important for chlamydial invasion.', *PLoS pathogens*, 6(7), p. e1000997. doi:
659 10.1371/journal.ppat.1000997.
660 **Jiwani, S., Alvarado, S., Ohr, R. J., Romero, A., Nguyen, B. and Jewett, T. J.** (2013)
661 '*Chlamydia trachomatis* Tarp Harbors Distinct G and F Actin Binding Domains That Bundle Actin
662 Filaments', *Journal of Bacteriology*, 195(4), pp. 708–716. doi: 10.1128/JB.01768-12.
663 **Kanchanawong, P., Shtengel, G., Pasapera, A. M., Ramko, E. B., Davidson, M. W., Hess,**
664 **H. F. and Waterman, C. M.** (2010) 'Nanoscale architecture of integrin-based cell adhesions',
665 *Nature*, 468(7323), pp. 580–584. doi: 10.1038/nature09621.
666 **Kim, M., Ogawa, M., Fujita, Y., Yoshikawa, Y., Nagai, T., Koyama, T., Nagai, S., Lange, A.,**
667 **Fässler, R. and Sasakawa, C.** (2009) 'Bacteria hijack integrin-linked kinase to stabilize focal
668 adhesions and block cell detachment.', *Nature*, 459(7246), pp. 578–82. doi:
669 10.1038/nature07952.
670 **Kim, M., Ogawa, M., Mimuro, H. and Sasakawa, C.** (2010) 'Reinforcement of epithelial cell
671 adhesion to basement membrane by a bacterial pathogen as a new infectious stratagem',
672 *Virulence*, 1(April 2010), pp. 52–55. doi: 10.1038/nature07952.he.
673 **Kumar, R., Gong, H., Liu, L., Ramos-Solis, N., Seye, C. I. and Derbigny, W. A.** (2019) 'TLR3
674 deficiency exacerbates the loss of epithelial barrier function during genital tract *Chlamydia*
675 *muridarum* infection.', *PloS one*. Edited by G. Zhong, 14(1), p. e0207422. doi:
676 10.1371/journal.pone.0207422.

677 **Kumar, Y. and Valdivia, R. H.** (2008) 'Reorganization of the host cytoskeleton by the
678 intracellular pathogen *Chlamydia trachomatis*', *Commun Integr Biol*, 1(2), pp. 175–177. doi:
679 10.1016/j.chom.2008.05.018.www.landesbioscience.com.
680 **Kuwabara, T., Perkins, D. G. and Cogan, D. G.** (1976) 'Sliding of the epithelium in
681 experimental corneal wounds.', *Investigative ophthalmology*, 15(1), pp. 4–14. Available at:
682 http://www.ncbi.nlm.nih.gov/pubmed/1245378 (Accessed: 27 November 2019).
683 **Lacy, H. M., Bowlin, A. K., Hennings, L., Scurlock, A. M., Nagarajan, U. M. and Rank, R. G.**
684 (2011) 'Essential role for neutrophils in pathogenesis and adaptive immunity in *Chlamydia*
685 *caviae* ocular infections.', *Infection and immunity*. Edited by J. N. Weiser, 79(5), pp. 1889–97.
686 doi: 10.1128/IAI.01257-10.
687 **Lane, B. J., Mutchler, C., Al Khodor, S., Grieshaber, S. S. and Carabeo, R. A.** (2008)
688 'Chlamydial entry involves TARP binding of guanine nucleotide exchange factors.', *PLoS*
689 *pathogens*, 4(3), p. e1000014. Available at: http://www.ncbi.nlm.nih.gov/pubmed/18383626
690 (Accessed: 22 November 2016).
691 **Laukaitis, C. M., Webb, D. J., Donais, K. and Horwitz, A. F.** (2001) 'Differential dynamics of
692 alpha 5 integrin, paxillin, and alpha-actinin during formation and disassembly of adhesions in
693 migrating cells.', *The Journal of cell biology*, 153(7), pp. 1427–40. doi: 10.1083/jcb.153.7.1427.
694 **Liu, Z., van Grunsven, L. A., Van Rossen, E., Schroyen, B., Timmermans, J.-P., Geerts, A.**
695 **and Reynaert, H.** (2010) 'Blebbistatin inhibits contraction and accelerates migration in mouse
696 hepatic stellate cells.', *British journal of pharmacology*, 159(2), pp. 304–15. doi: 10.1111/j.1476-
697 5381.2009.00477.x.
698 **Lutter, E. I., Bonner, C., Holland, M. J., Suchland, R. J., Stamm, W. E., Jewett, T. J.,**
699 **McClarty, G. and Hackstadt, T.** (2010) 'Phylogenetic Analysis of *Chlamydia trachomatis* Tarp
700 and Correlation with Clinical Phenotype', *Infection and Immunity*, 78(9), pp. 3678–3688. doi:
701 10.1128/IAI.00515-10.
702 **Marg, S., Winkler, U., Sestu, M., Himmel, M., Schönherr, M., Bär, J., Mann, A., Moser, M.,**

703 **Mierke, C. T., Rottner, K., Blessing, M., Hirrlinger, J. and Ziegler, W. H.** (2010) 'The vinculin-
704 DeltaIn20/21 mouse: characteristics of a constitutive, actin-binding deficient splice variant of
705 vinculin.', *PloS one*. Edited by D. P. Martin, 5(7), p. e11530. doi: 10.1371/journal.pone.0011530.
706 **Mehlitz, A., Banhart, S., Mäurer, A. P., Kaushansky, A., Gordus, A. G., Zielecki, J.,**
707 **Macbeath, G. and Meyer, T. F.** (2010) 'Tarp regulates early Chlamydia-induced host cell
708 survival through interactions with the human adaptor protein SHC1.', *The Journal of cell biology*,
709 190(1), pp. 143–57. doi: 10.1083/jcb.200909095.
710 **Morita-Ishihara, T., Miura, M., Iyoda, S., Izumiya, H., Watanabe, H., Ohnishi, M. and**
711 **Terajima, J.** (2013) 'EspO1-2 regulates EspM2-mediated RhoA activity to stabilize formation of
712 focal adhesions in enterohemorrhagic Escherichia coli-infected host cells.', *PloS one*. Edited by
713 F. Börnke, 8(2), p. e55960. doi: 10.1371/journal.pone.0055960.
714 **Mysorekar, I. U., Mulvey, M. A., Hultgren, S. J. and Gordon, J. I.** (2002) 'Molecular regulation
715 of urothelial renewal and host defenses during infection with uropathogenic Escherichia coli.',
716 *The Journal of biological chemistry*, 277(9), pp. 7412–9. doi: 10.1074/jbc.M110560200.
717 **Nagano, M., Hoshino, D., Koshikawa, N., Akizawa, T. and Seiki, M.** (2012) 'Turnover of
718 Focal Adhesions and Cancer Cell Migration', *International Journal of Cell Biology*, 2012, pp. 1–
719 10. doi: 10.1155/2012/310616.
720 **O'Connell, C. M., Ionova, I. A., Quayle, A. J., Visintin, A. and Ingalls, R. R.** (2006)
721 'Localization of TLR2 and MyD88 to *Chlamydia trachomatis* inclusions. Evidence for signaling
722 by intracellular TLR2 during infection with an obligate intracellular pathogen.', *The Journal of*
723 *biological chemistry*, 281(3), pp. 1652–9. doi: 10.1074/jbc.M510182200.
724 **Pan, Q., Zhang, Q., Chu, J., Pais, R., Liu, S., He, C. and Eko, F. O.** (2017) '*Chlamydia*
725 *abortus* Pmp18.1 Induces IL-1β Secretion by TLR4 Activation through the MyD88, NF-κB, and
726 Caspase-1 Signaling Pathways.', *Frontiers in cellular and infection microbiology*, 7, p. 514. doi:
727 10.3389/fcimb.2017.00514.
728 **Pasapera, A. M., Schneider, I. C., Rericha, E., Schlaepfer, D. D. and Waterman, C. M.**

729 (2010) ‘Myosin II activity regulates vinculin recruitment to focal adhesions through FAK-
730 mediated paxillin phosphorylation.’, *The Journal of cell biology*, 188(6), pp. 877–90. doi:
731 10.1083/jcb.200906012.
732 **Pijuan, J., Barceló, C., Moreno, D. F., Maiques, O., Sisó, P., Marti, R. M., Macià, A. and**
733 **Panosa, A.** (2019) ‘In vitro Cell Migration, Invasion, and Adhesion Assays: From Cell Imaging to
734 Data Analysis.’, *Frontiers in cell and developmental biology*, 7, p. 107. doi:
735 10.3389/fcell.2019.00107.
736 **Ramsey, K. H., Sigar, I. M., Schripsema, J. H., Shaba, N. and Cohoon, K. P.** (2005)
737 ‘Expression of matrix metalloproteinases subsequent to urogenital *Chlamydia muridarum*
738 infection of mice.’, *Infection and immunity*, 73(10), pp. 6962–73. doi: 10.1128/IAI.73.10.6962-
739 6973.2005.
740 **Rosenblatt, J., Raff, M. C. and Cramer, L. P.** (2001) ‘An epithelial cell destined for apoptosis
741 signals its neighbors to extrude it by an actin- and myosin-dependent mechanism’, *Current*
742 *Biology*, 11(23), pp. 1847–1857. doi: 10.1016/S0960-9822(01)00587-5.
743 **Schindelin, J., Arganda-Carreras, I., Frise, E., Kaynig, V., Longair, M., Pietzsch, T.,**
744 **Preibisch, S., Rueden, C., Saalfeld, S., Schmid, B., Tinevez, J.-Y., White, D. J.,**
745 **Hartenstein, V., Eliceiri, K., Tomancak, P. and Cardona, A.** (2012) ‘Fiji: an open-source
746 platform for biological-image analysis.’, *Nature methods*, 9(7), pp. 676–82. doi:
747 10.1038/nmeth.2019.
748 **Schneider, C. A., Rasband, W. S. and Eliceiri, K. W.** (2012) ‘NIH Image to ImageJ: 25 years
749 of image analysis’, *Nature Methods*, 9(7), pp. 671–675. doi: 10.1038/nmeth.2089.
750 **Shames, S. R., Deng, W., Guttman, J. A., de Hoog, C. L., Li, Y., Hardwidge, P. R., Sham, H.**
751 **P., Vallance, B. A., Foster, L. J. and Finlay, B. B.** (2010) ‘The pathogenic E. coli type III
752 effector EspZ interacts with host CD98 and facilitates host cell prosurvival signalling.’, *Cellular*
753 *microbiology*, 12(9), pp. 1322–39. doi: 10.1111/j.1462-5822.2010.01470.x.
754 **Shaw, J. L. V, Wills, G. S., Lee, K.-F., Horner, P. J., McClure, M. O., Abrahams, V. M.,**

Wheelhouse, N., Jabbour, H. N., Critchley, H. O. D., Entrican, G. and Horne, A. W. (2011) '*Chlamydia trachomatis* infection increases fallopian tube PROKR2 via TLR2 and NFκB activation resulting in a microenvironment predisposed to ectopic pregnancy.', *The American journal of pathology*, 178(1), pp. 253–60. doi: 10.1016/j.ajpath.2010.11.019.

Shtengel, G., Galbraith, J. A., Galbraith, C. G., Lippincott-Schwartz, J., Gillette, J. M., Manley, S., Sougrat, R., Waterman, C. M., Kanchanawong, P., Davidson, M. W., Fetter, R. D. and Hess, H. F. (2009) 'Interferometric fluorescent super-resolution microscopy resolves 3D cellular ultrastructure.', *Proc Natl Acad Sci U S A*, 106(9), pp. 3125–30. doi: 10.1073/pnas.0813131106.

Smilenov, L. B., Mikhailov, A., Pelham, R. J., Marcantonio, E. E. and Gundersen, G. G. (1999) 'Focal Adhesion Motility Revealed in Stationary Fibroblasts', *Science*, 286(5442), pp. 1172–1174. doi: 10.1126/science.286.5442.1172.

Straight, A. F., Cheung, A., Limouze, J., Chen, I., Westwood, N. J., Sellers, J. R. and Mitchison, T. J. (2003) 'Dissecting temporal and spatial control of cytokinesis with a myosin II Inhibitor.', *Science (New York, N.Y.)*, 299(5613), pp. 1743–7. doi: 10.1126/science.1081412.

Thwaites, T., Nogueira, A. T., Campeotto, I., Silva, A. P., Grieshaber, S. S. and Carabeo, R. A. (2014) 'The *Chlamydia* Effector TarP Mimics the Mammalian Leucine-Aspartic Acid Motif of Paxillin to Subvert the Focal Adhesion Kinase during Invasion', *Journal of Biological Chemistry*, 289(44), pp. 30426–30442. doi: 10.1074/jbc.M114.604876.

Thwaites, T. R., Pedrosa, A. T., Peacock, T. P. and Carabeo, R. A. (2015) 'Vinculin Interacts with the *Chlamydia* Effector TarP Via a Tripartite Vinculin Binding Domain to Mediate Actin Recruitment and Assembly at the Plasma Membrane', *Frontiers in Cellular and Infection Microbiology*. Frontiers, 5, p. 88. doi: 10.3389/fcimb.2015.00088.

Vossenkämper, A., Macdonald, T. T. and Marchès, O. (2011) 'Always one step ahead: How pathogenic bacteria use the type III secretion system to manipulate the intestinal mucosal immune system.', *Journal of inflammation (London, England)*, 8(1), p. 11. doi: 10.1186/1476-

781 9255-8-11.

782 **Wang, H. H., Tanaka, H., Qin, X., Zhao, T., Ye, L.-H., Okagaki, T., Katayama, T., Nakamura,**
783 **A., Ishikawa, R., Thatcher, S. E., Wright, G. L. and Kohama, K.** (2008) 'Blebbistatin inhibits
784 the chemotaxis of vascular smooth muscle cells by disrupting the myosin II-actin interaction.',
785 *American journal of physiology. Heart and circulatory physiology*, 294(5), pp. H2060-8. doi:
786 10.1152/ajpheart.00970.2007.

787 **Zaidel-Bar, R., Itzkovitz, S., Ma'ayan, A., Iyengar, R. and Geiger, B.** (2007) 'Functional atlas
788 of the integrin adhesome.', *Nature cell biology*, 9(8), pp. 858–67. doi: 10.1038/ncb0807-858.

789

790

791 **Figure legends**

792 **Figure 1. *C. trachomatis*-infected Cos7 cells exhibit increased focal adhesion numbers.**
793 (A) Cos7 cells infected with the indicated chlamydial strain/species or mock-infected were
794 monitored at 24 hpi, and focal adhesions visualized by immunostaining for paxillin.

795

796 **Figure 2. Infection-dependent increase in focal adhesion numbers requires *de novo***
797 **chlamydial protein synthesis.** (A) Cos7 cells infected with *C. trachomatis* serovar L2 were
798 mock- or chloramphenicol-treated at the start of infection for either 8 or 20 h. Focal adhesions
799 were visualized by immunostaining for paxillin (green). Scale bar length 10μm. (B) Focal
800 adhesions were counted using the particle tracker plug-in in NIH ImageJ. Analysis revealed a
801 lack of effect of the 8-h Cm treatment on FA numbers, while the 24-h treatment yielded a
802 statistically significant decreasein FA numbers. Data are represented as box-and-whisker plots.
803 Whiskers represent the lowest and highest data point still within 1.5 times the interquartile
804 range. The light blue asterisks indicate significant difference relative to the mock-infected control
805 (Wilcoxon rank sum test * = $p<0.05$). The black cross shows the average for each experimental
806 sample.

807

808 **Figure 3. Focal adhesions of *Chlamydia* infected cells are resistant to blebbistatin.** Cos7
809 cells were mock-infected or infected with CtrL2 for 24 h or 8 h. Cells were fixed and stained for
810 the focal adhesion marker paxillin (green), F-actin (red) and human convalescent serum for *C.*
811 *trachomatis* (white). Cells were also mock- or pre-treated with chloramphenicol (Cm) followed by

812 infection of live EBs. Cm treatment was maintained for the duration of the experiment.
813 Blebbistatin 10 μM was introduced during the last hour of infection. Cells without blebbistatin
814 treatment showed clear F-actin stress fibres and paxillin-labeled focal adhesions. While both
815 structures were lost in mock-infected cells, infected cells retained the focal adhesions. This
816 characteristic was sensitive to Cm inhibition of *de novo* chlamydial protein synthesis. Scale bar
817 = 10μm.
818
819 **Figure 4. The type III effector TarP localizes to focal adhesions during *Chlamydia***
820 **infection.** (A) CtrL2-infected MEF cells were immunostained for a rabbit polyclonal antibody to
821 TarP and a mouse monoclonal antibody to talin. Inclusions were visualized by staining with
822 DAPI. TarP localized to talin-positive FAs (arrowheads) in infected, but not in mock-infected
823 controls. Scale bar = 10μm.
824
825 **Figure 5. The focal adhesion localization of TarP requires its LDVBD domain and the host**
826 **protein vinculin, but not FAK.** (A) Representation of *C. trachomatis* effector protein TarP and
827 its known domains fused to mTurquoise2 fluorescent protein. (B) Wild type or vinculin-knockout
828 MEFs were transfected with different mTurquoise2-tagged TarP constructs (green) and imaged
829 by confocal microscopy to evaluate colocalization with paxillin (red) at focal adhesions.
830 Phalloidin was used to stain F-actin (blue). Cells were transfected for 20 h, at which time the
831 cells were fixed and processed for immunofluorescence staining for paxillin. (C) In a parallel
832 experiment, wild type and FAK1-deficient MEFs were transfected to express Flag-HA-LDVBD
833 and stained for flag (green). Colocalization with paxillin (red) was assessed by confocal
834 microscopy. (D) Ectopically expressed LDVBD localizes to β1-integrin and paxillin-positive focal
835 adhesions. Scale bar = 10μm.
836
837 **Figure 6. The ectopic expression of TarP LDVBD is sufficient to increase focal adhesion**
838 **numbers.** (A) Cos7 cells expressing different deletion derivatives of TarP or vector only were
839 processed for immunofluorescence with anti-paxillin antibody to visualize focal adhesions.
840 Representative images are shown. Scale bar = 10 μm. (B) Focal adhesion numbers were
841 counted using the particle counting plug-in in NIH ImageJ. Data are focal adhesion number per
842 cell and illustrated as box-whisker plot. Whiskers represent the lowest and highest data point
843 still within 1.5 times the interquartile range. For statistical analyses the Wilcoxon Rank sum test
844 was used to determine significance when compared to vector-only control (* = $p<0.05$).
845

846 **Figure 7. The LDVBD domain of TarP and the host protein vinculin are required for focal**
847 **adhesion resistance to blebbistatin treatment.** (A) Wild type or vinculin-knockout MEFs were
848 infected with C. trachomatis serovar L2. Cells at 24 hpi were mock-treated or treated for 60 min
849 with 10 μM of blebbistatin. The cells were then processed for immunofluorescence staining for
850 paxillin (green) and actin (red). Retention or loss of focal adhesions were monitored. Focal
851 adhesions were only resistant to blebbistatin-induced disassembly if the cell was infected and
852 expressing vinculin. (B) In a parallel experiment, wild type or vinculin-knockout MEFs were
853 transfected for 20 h with the empty vector or LDVBD-mTurquoise2 fusion protein. During the
854 last hour, cells were either mock- or blebbistatin-treated. Cells were processed to visualize
855 paxillin (red), LDVBD (green), and actin (blue; shown in composite images). LDVBD was
856 sufficient to confer resistance to blebbistatin-induced disassembly to focal adhesions.
857 Resistance also required vinculin. Scale bar = 10 μm.
858
859 **Figure 8. TarP-targeted focal adhesions display altered nanoscale architecture.** (A) Cos7
860 cells pre-transfected with paxillin-tdEos, FAK-TdEos, or Vinculin-TdEos, and grownon gold
861 fiducial coverslips were mock- or C. trachomatis-infected for 24 h. The cells were fixed and
862 processed for iPALM imaging. Representative images are shown. For each sample, multiple
863 panels are provided. The top panel shows the top view of area around the focal adhesion of
864 interest (white border). The middle panel displays a top view of the focal adhesion indicated by
865 the white border. The bottom panel shows the side view and corresponding z histograms. Note
866 the significant shifts in paxillin and FAK localization, but not vinculin. (B) Cos7 cells were co-
867 transfected with paxillin-tdEos and either TarP ΔPRD or LDVBD only by electroporation. The
868 cells were seeded on gold fiducial coverslips, and processed for iPALM at 20 h post-
869 transfection. Description of each panel is as above in (A). Note the significant shift in the
870 location of paxillin within the TarP-positive focal adhesions. The various colors indicate the
871 distance (z-coordinates) from the gold fiducial marker, (e.g. z = 0 nm; red). Red scale bar =
872 1μm. White scale bar = 200 nm.
873
874 **Figure 9. The LDVBD domain of TarP is sufficient to inhibit cell migration.** MEFs that were
875 mock-infected, Chlamydia-infected, vector-only-transfected, or LDVBD-transfected were seeded
876 within ibidi μ-slide live cell imaging chambers. Time-lapse imaging was performed every 10
877 minutes for 10 h to evaluate cell motility. (A) For analysis of the infection experiments, a 5-h
878 imaging window common to both mock- and *Chlamydia*-infected samples was chosen that
879 maximized the number of cells that remained within the field of view. Cells were tracked using

880 the manual tracking function in NIH ImageJ, and the cell trajectory was traced and plotted with
881 the starting points assigned to the origin. (B) Analysis of the transfection experiment was in a
882 common 10-h imaging window. Data were acquired and plotted as in (A). (C) Velocity and
883 Euclidean distance traveled were calculated for each cell from each experimental group. Values
884 were plotted as dot-plots with mean $\pm$ S.D. indicated by the bars. Statistical significance was
885 calculated using the Wilcoxon Rank Sum test. * indicates $p < 0.05$.

FIGURE 1

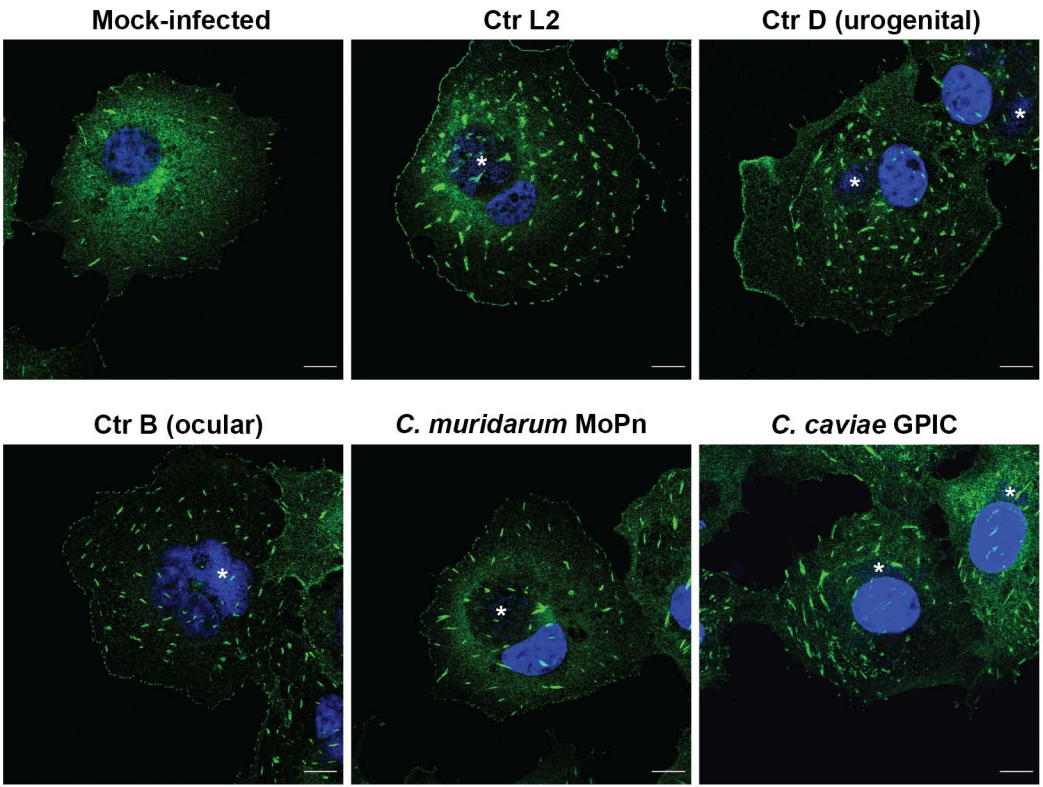
Mock-infected
Ctr L2
Ctr D (urogenital)
Ctr B (ocular)
C. muridarum MoPn
C. caviae GPIC

FIGURE 2

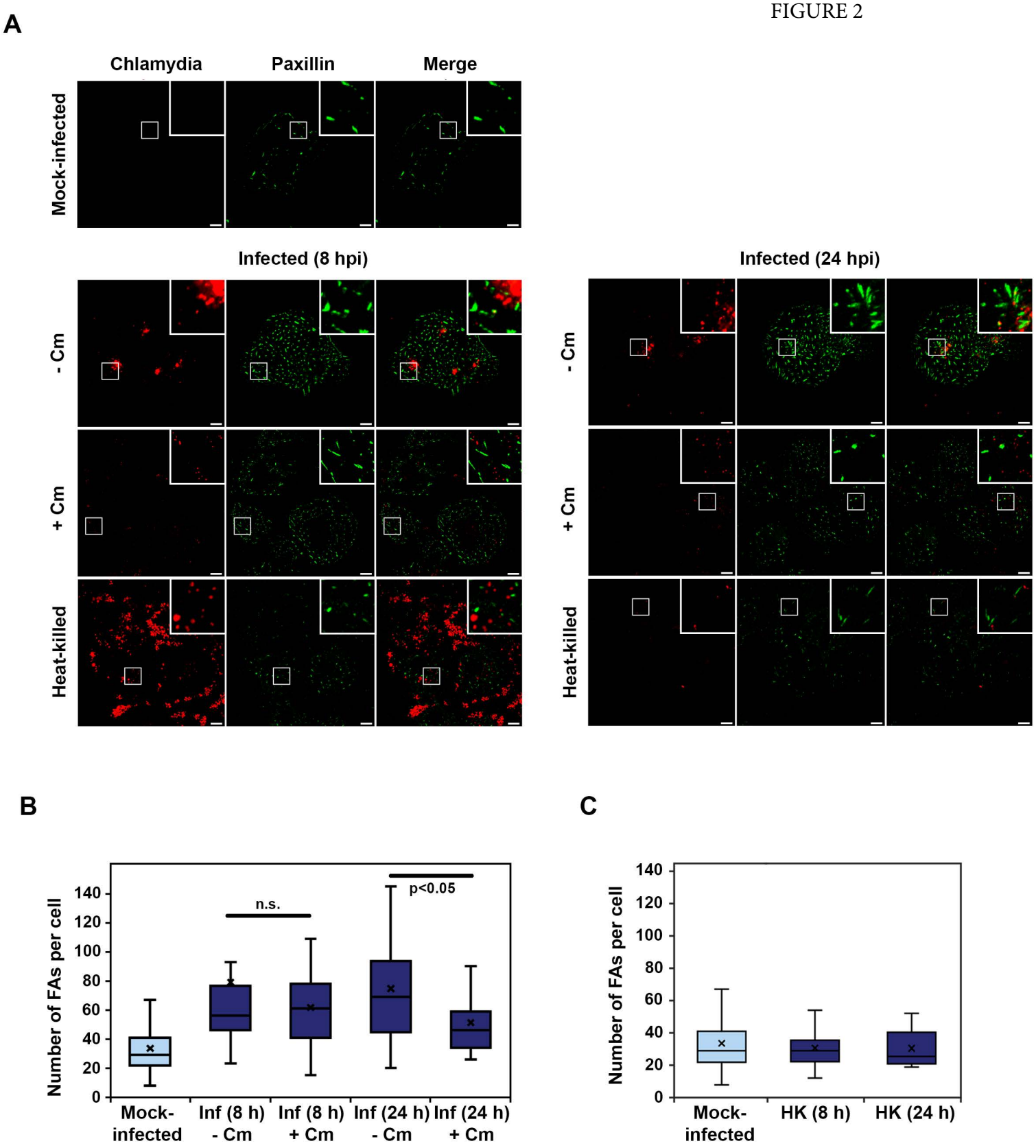
A
Chlamydia
Paxillin
Merge
Mock-infected
Infected (8 hpi)
Infected (24 hpi)
- Cm
+ Cm
Heat-killed
B
Number of FAs per cell
140
120
100
80
60
40
20
0
n.s.
p<0.05
Mock-infected
Inf (8 h) - Cm
Inf (8 h) + Cm
Inf (24 h) - Cm
Inf (24 h) + Cm
C
Number of FAs per cell
140
120
100
80
60
40
20
0
Mock-infected
HK (8 h)
HK (24 h)

FIGURE 3

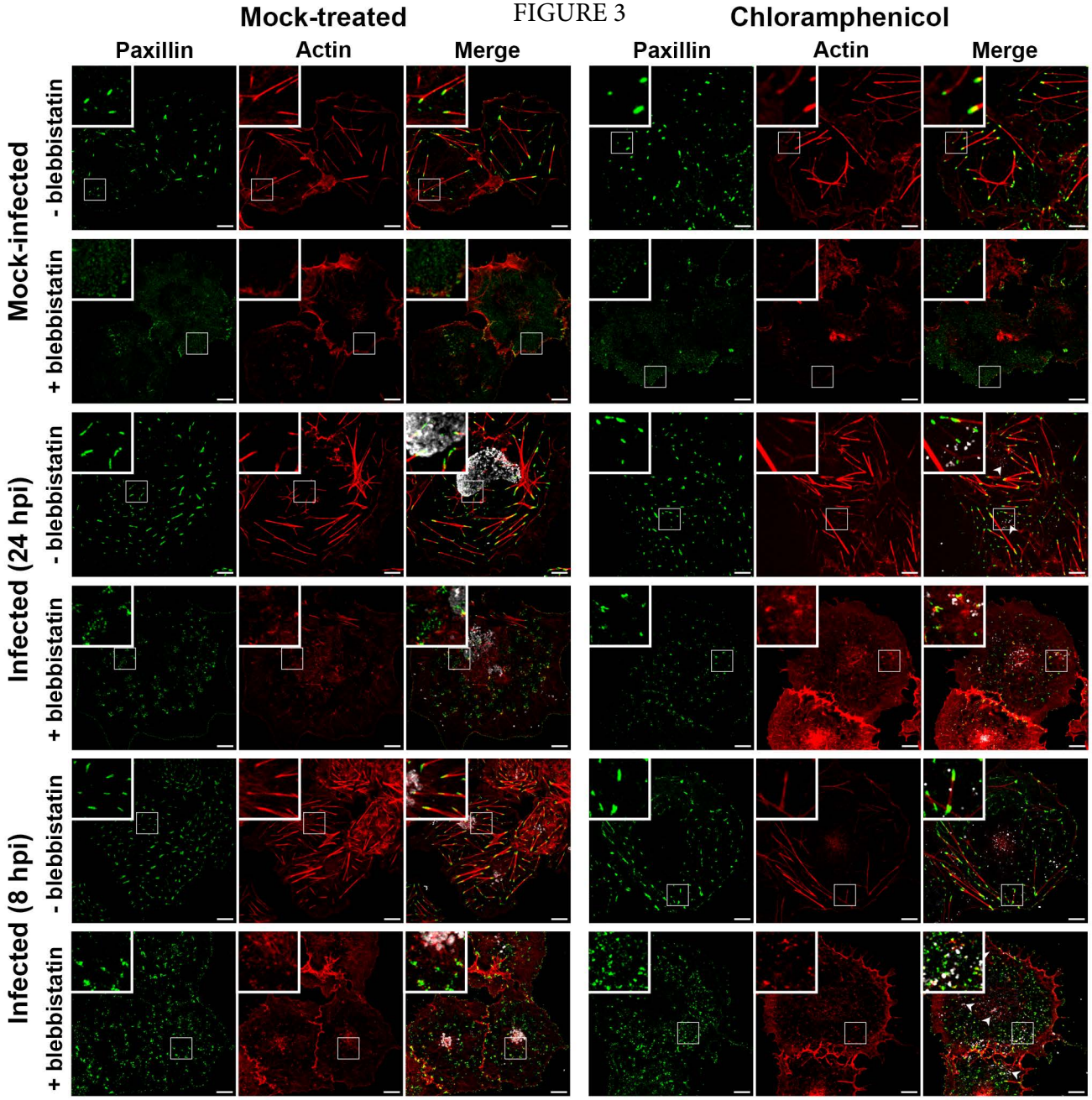
Mock-treated
Chloramphenicol
Paxillin
Actin
Merge
Paxillin
Actin
Merge
Mock-infected
- blebbistatin
+ blebbistatin
Infected (24 hpi)
- blebbistatin
+ blebbistatin
Infected (8 hpi)
- blebbistatin
+ blebbistatin

FIGURE 4

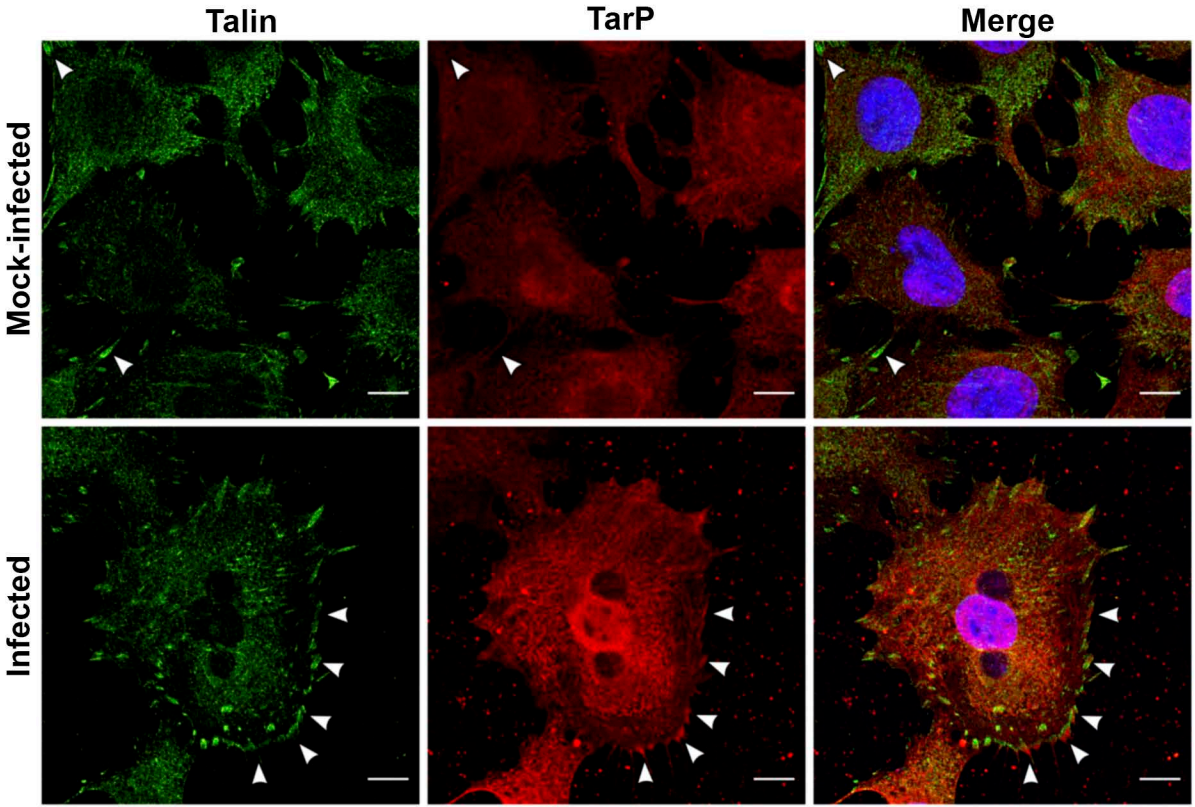

FIGURE 5

A

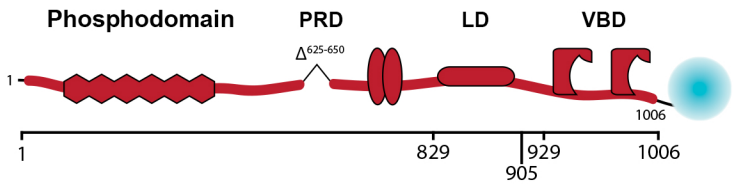

B

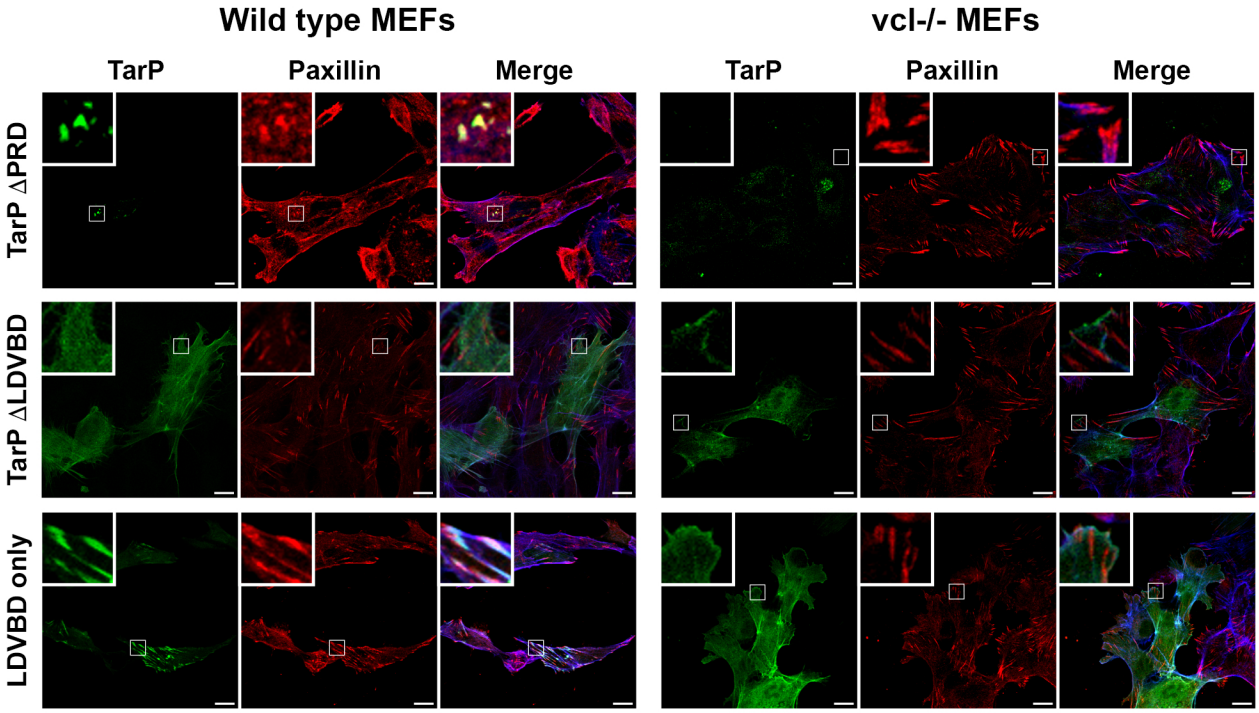

C

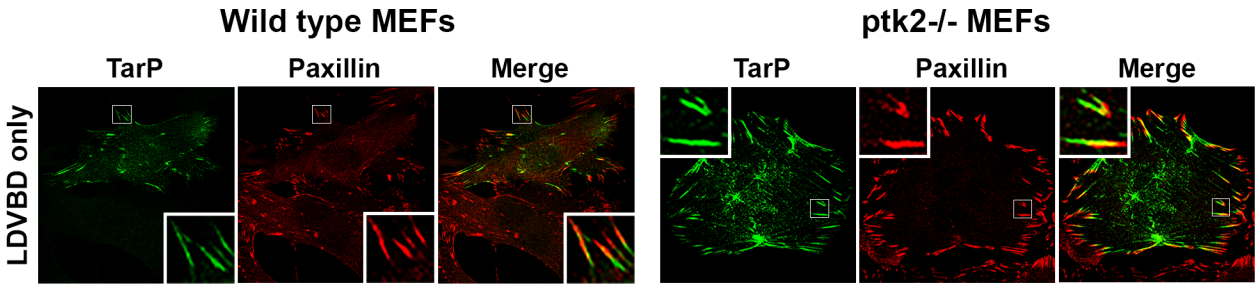

D

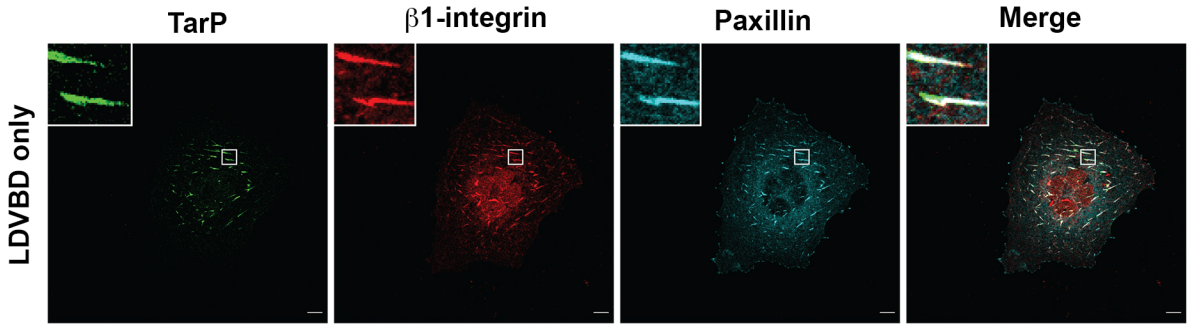

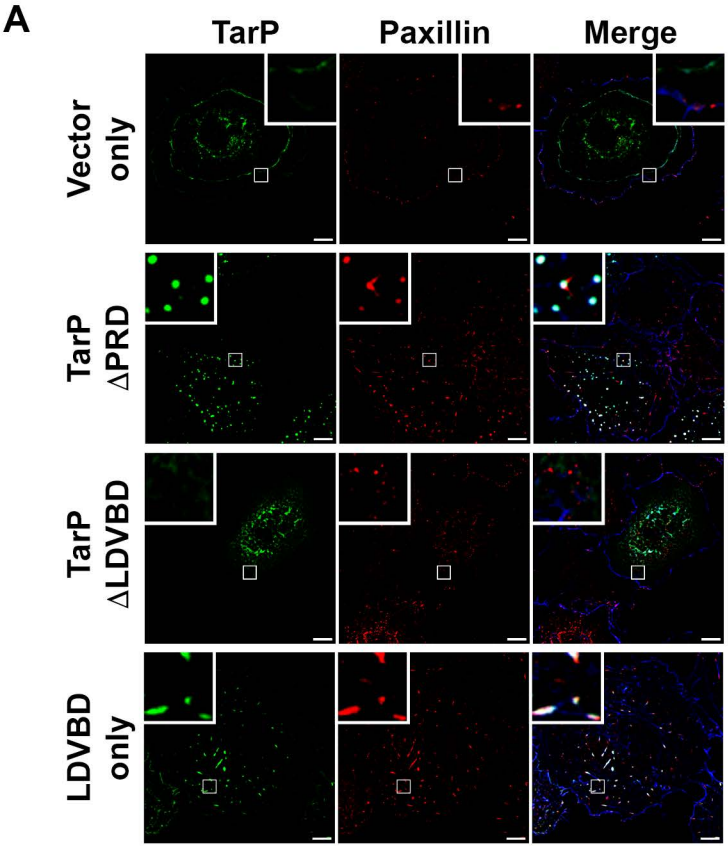
A
TarP
Paxillin
Merge
Vector only
TarP ΔPRD
TarP ΔLDVBD
LDVBD only

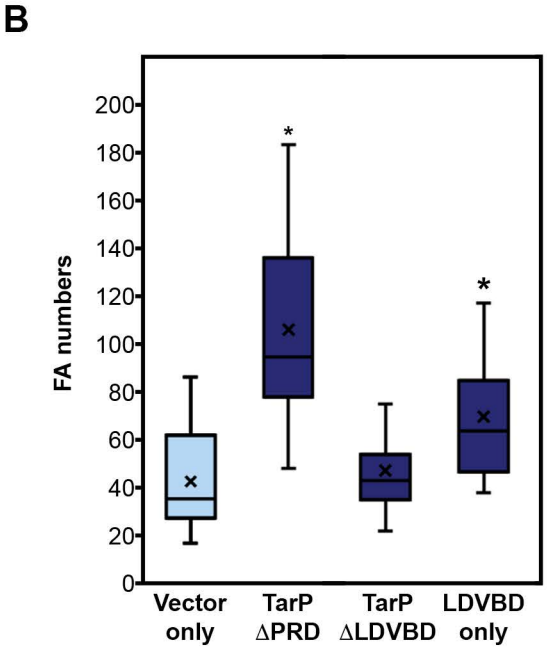
B
FA numbers
0
20
40
60
80
100
120
140
160
180
200
*
*
Vector only
TarP ΔPRD
TarP ΔLDVBD
LDVBD only

FIGURE 6

FIGURE 7

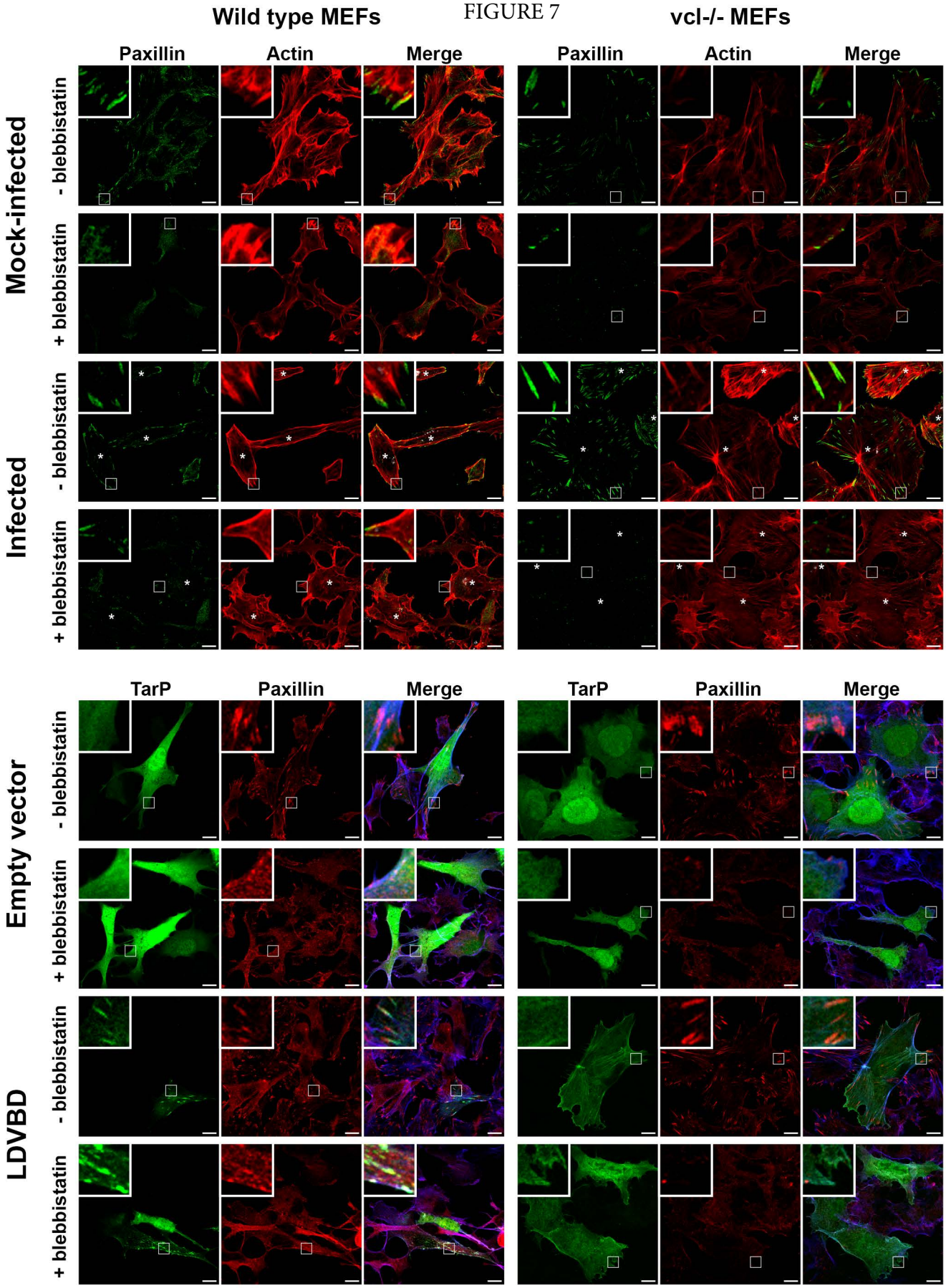
Wild type MEFs
vcl-/- MEFs
Paxillin
Actin
Merge
Paxillin
Actin
Merge
Mock-infected
- blebbistatin
+ blebbistatin
Infected
- blebbistatin
+ blebbistatin
TarP
Paxillin
Merge
TarP
Paxillin
Merge
Empty vector
- blebbistatin
+ blebbistatin
LDVBD
- blebbistatin
+ blebbistatin

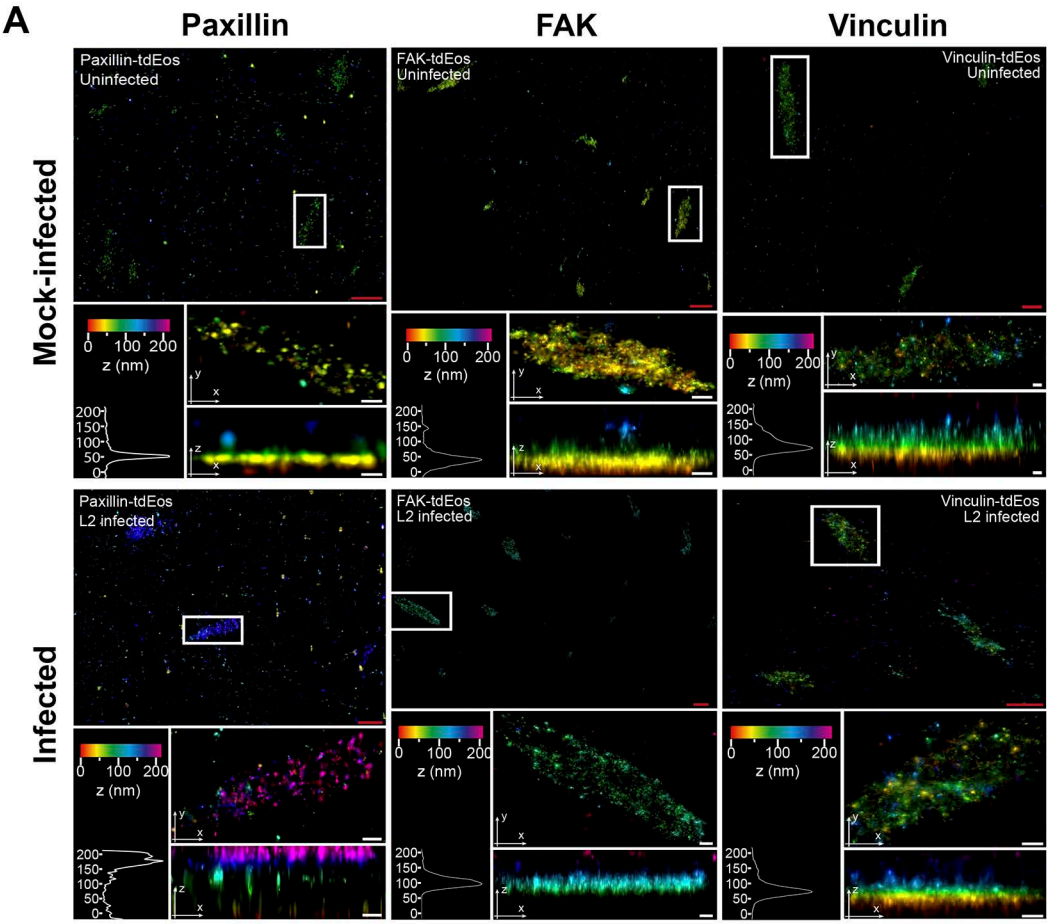
A
Paxillin
FAK
Vinculin
Mock-infected
Infected
Paxillin-tdEos
Uninfected
FAK-tdEos
Uninfected
Vinculin-tdEos
Uninfected
Paxillin-tdEos
L2 infected
FAK-tdEos
L2 infected
Vinculin-tdEos
L2 infected
0 100 200
z (nm)
200
150
100
50
0
y
x
z

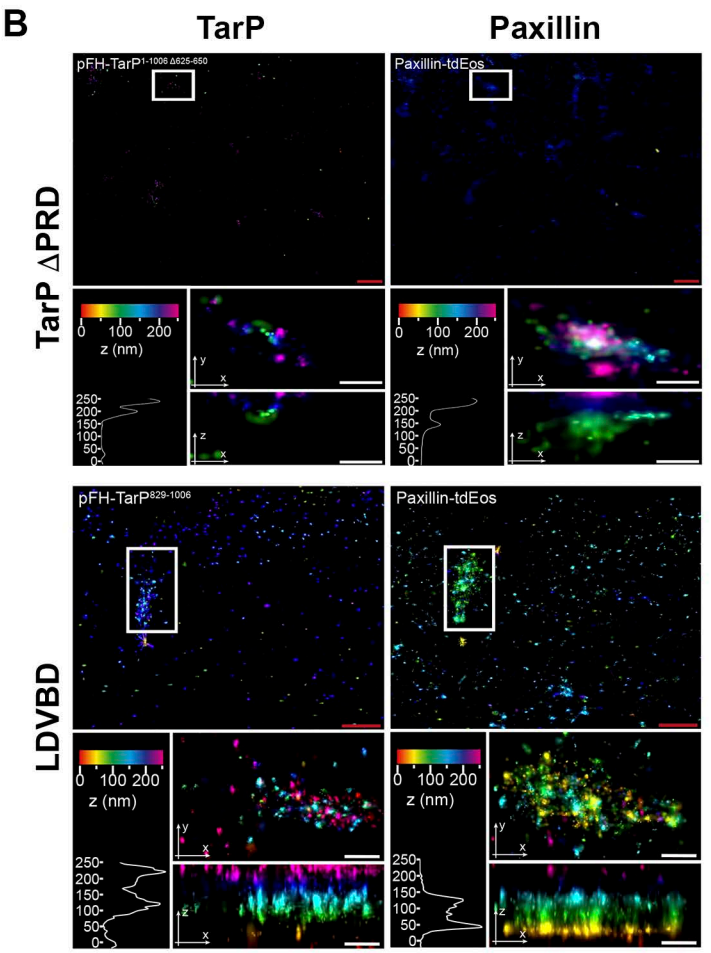
B
TarP
Paxillin
TarP ΔPRD
LDVBD
pFH-TarP1-1006 Δ625-650
Paxillin-tdEos
pFH-TarP829-1006
Paxillin-tdEos
0 100 200
z (nm)
250
200
150
100
50
0
y
x
z

FIGURE 8

FIGURE 9

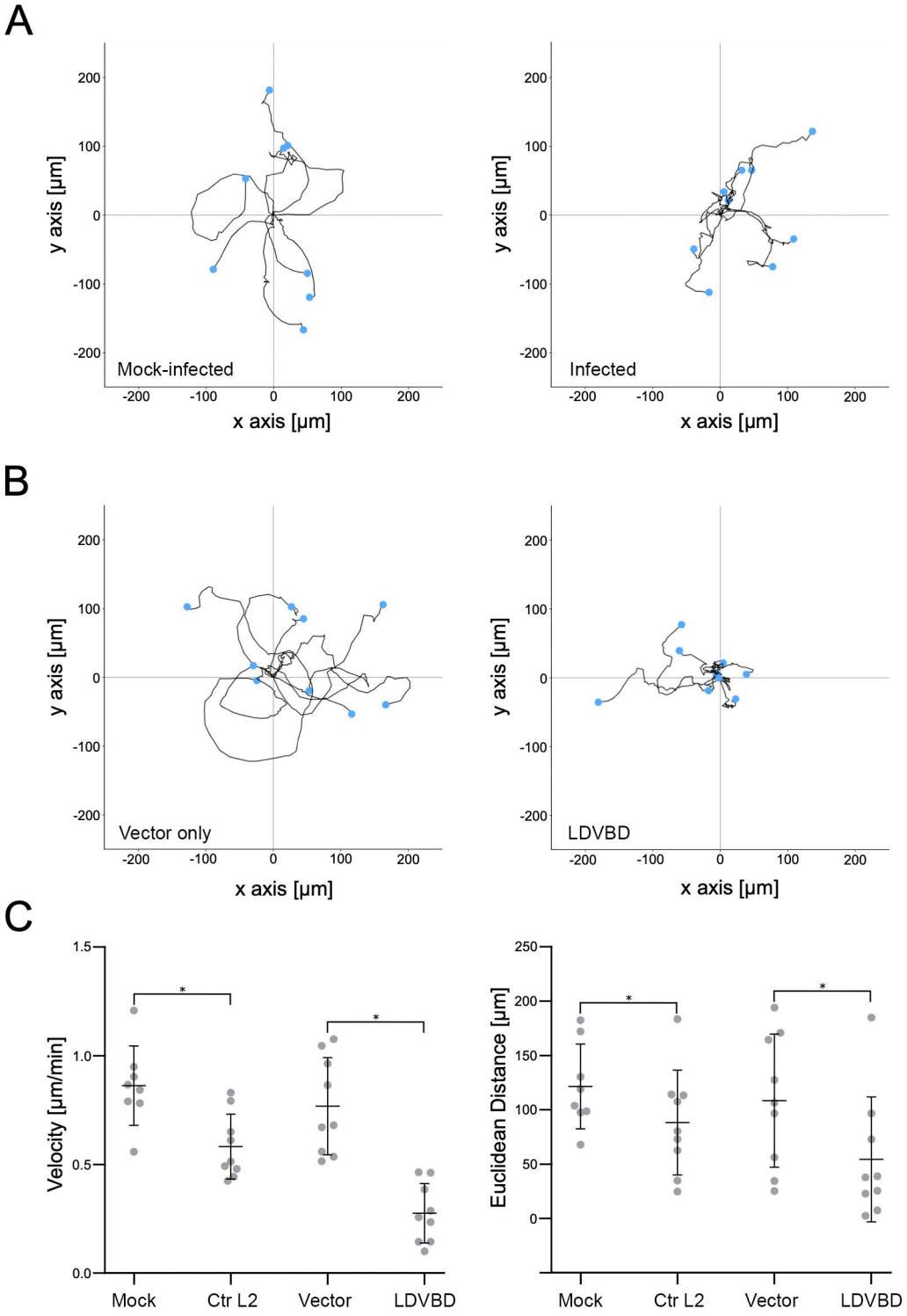
A
Mock-infected
Infected
y axis [µm]
x axis [µm]
B
Vector only
LDVBD
C
Velocity [µm/min]
Euclidean Distance [µm]
Mock
Ctr L2
Vector
LDVBD
*

Supplemental Table 1 - Primers used in this study

Primer number	Primer name	Primer sequence 5' to 3'
1	Fwd-TarP	GCATGGTACCATGACGAATTCTATATCAGGTG
2	Rev-VBD domain	TAATGGATCCGGGTATCCTACGGTATCAATC
3	Rev- TarP$^{1\text{-}829\Delta 625\text{-}650}$	TAATGGATCCCTTGGAGGTGGTGAAGG
4	Fwd-VBD domain	TAATGGTACCATGAACAAATTCCGCAAAGAA
5	Fwd-LD domain	TAATGGTACCATGACCCCATCAACTACAACA
6	Rev-LD domain	TAATGGATCCATAGATCCCGGCTTGCC
7	FWD-TarPΔ$^{625\text{-}650}$	ATGGCATTGTCAATGTCAACGTTGGC
8	Rev-TarPΔ$^{625\text{-}650}$	ACATTGAAATGCCATCGTCTTCGCT
9	Fwd-TarP-FH	AACGGCCGCCAGTGTATGACGAATTCTATATCAGGTG ATCAACCT
10	Rev-TarP-FH	CCCTCTAGATGCATGTTATCCTACGGTATCAATCAGT GAGCTT
11	Fwd-FH-TarP	GATACCGTAGGATAACATGCATCTAGAGGGCCCTATT CTATAG
12	Rev-FH-TarP	TATAGAATTCGTCATACACTGGCGGCCGTTACTA
13	Fwd-TarP$^{829\text{-}1006}$-FH	AACGGCCGCCAGTGTACCCCATCAACTACAACATTAA GAACG
14	Rev- TarP$^{829\text{-}1006}$-FH	CCCTCTAGATGCATGTCCTACGGTATCAATCAGTGAG CTTAG
15	Fwd-FH- TarP$^{829\text{-}1006}$	ATTGATACCGTAGGACATGCATCTAGAGGGCCCTATT CTATAG
16	Rev-FH- TarP$^{829\text{-}1006}$	TGTAGTTGATGGGGTACACTGGCGGCCGTTACTA
17	Rev-TarP$^{1\text{-}829\Delta 625\text{-}650}$-FH	CCCTCTAGATGCATGTTATGGAGGTGGTGAAGGCAG TAG
18	Fwd-FH- TarP$^{1\text{-}829\Delta 625\text{-}650}$	CCTTCACCACCTCCATAACATGCATCTAGAGGGCCCT ATTCTATAG

Figure S1. TarP translocated by *C. trachomatis* is stable. (A) Cos7 cells were either mock-infected or *Chlamydia*-infected for the indicated times, and maintained throughout in the presence of the prokaryotic protein synthesis inhibitor chloramphenicol. Whole cell lysates were harvested to monitor by Western blot the presence and stability of translocated TarP proteins. A rabbit polyclonal anti-TarP antibody was used. Protein concentrations were determined and adjusted to ensure equal loading. β-tubulin was used as the loading control. Mock-infected and EB-only samples were added to demonstrate specificity of the anti-TarP antibody used.

Figure S2. The PRD domain of TarP is not required for focal adhesion localization upon ectopic expression. Full-length TarP and TarP ΔPRD, both fused to mTurquoise2 were expressed ectopically in wild type MEFs for 19 h. The cells were processed for immunostaining for paxillin to visualize focal adhesions. Both full-length TarP and TarP ΔPRD colocalized with paxillin-positive structures, with the forming forming larger protein aggregates (arrowheads). Smaller TarP-positive punctae are indicated by white arrows.

Figure S3. Infection disrupts the stratified organization of focal adhesions. Cos7 cells were either mock-infected or infected with *C. trachomatis* serovar L2 for 20 h. DIC images of cells analyzed by iPALM were acquired to demonstrate the infection state. Regions of interests are bounded by white lines, and inclusions indicated by arrowheads.

Figure S4. LDVBD-expressing cells exhibited restricted motility relative to the empty vector-transfected control cells. Acquisition of the fluorescent channel was limited to the final frame of the motility assay to minimize phototoxicity. Images show the final DIC and fluorescent channel captured following 10 hours of time-lapse imaging. The DIC channel includes the dot and line overlay generated via ImageJ's manual tracking function to indicate the cell's movement over time.

Movie S1. Infection inhibits cell motility. A representative video assembled from a 17-h time-lapse imaging of mock-infected MEFs shows motility of individual cells with track outlines included.

Movie S2. Infection inhibits cell motility. A representative video assembled from a 17-h time-lapse imaging of *C. trachomatis*-infected MEFs shows motility of individual cells with track outlines included.

Movie S3. LDVBD is sufficient to inhibit cell motility. MEFs transfected with the vector alone was monitored for 17 h. A representative video assembled from a series of time-lapse images shows the degree of cell motility in the vector-only control group.

Movie S4. LDVBD is sufficient to inhibit cell motility. MEFs transfected with the LDVBD-mTurquoise2 was monitored for 17 h. A representative video assembled from a series of time-lapse images shows inhibition of cell motility of LDVBD-expressing cells.

Movie S5. *Chlamydia*-infected cells are resistant to detachment by mild trypsinization. Mock-infected HeLa cells growing on glass coverslips were treated by 0.025% Trypsin + EDTA, and imaged at 60-s intervals for 30 min. Note that the cells start to round up by seven min of incubation in trypsin.

Movie S6. *Chlamydia*-infected cells are resistant to detachment by mild trypsinization. *C. trachomatis* serovar L2-infected HeLa cells growing on glass coverslips were treated by 0.025% Trypsin + EDTA at 24 h post-infection, and imaged at 60-s intervals for 30 min. In contrast to

mock-infected cells shown in Movie S5, the infected cells remained attached and spread out after 30 min of mild trypsinization, indicating a possible enhancement of adhesion of infected cells to the substrate.

FIGURE S1

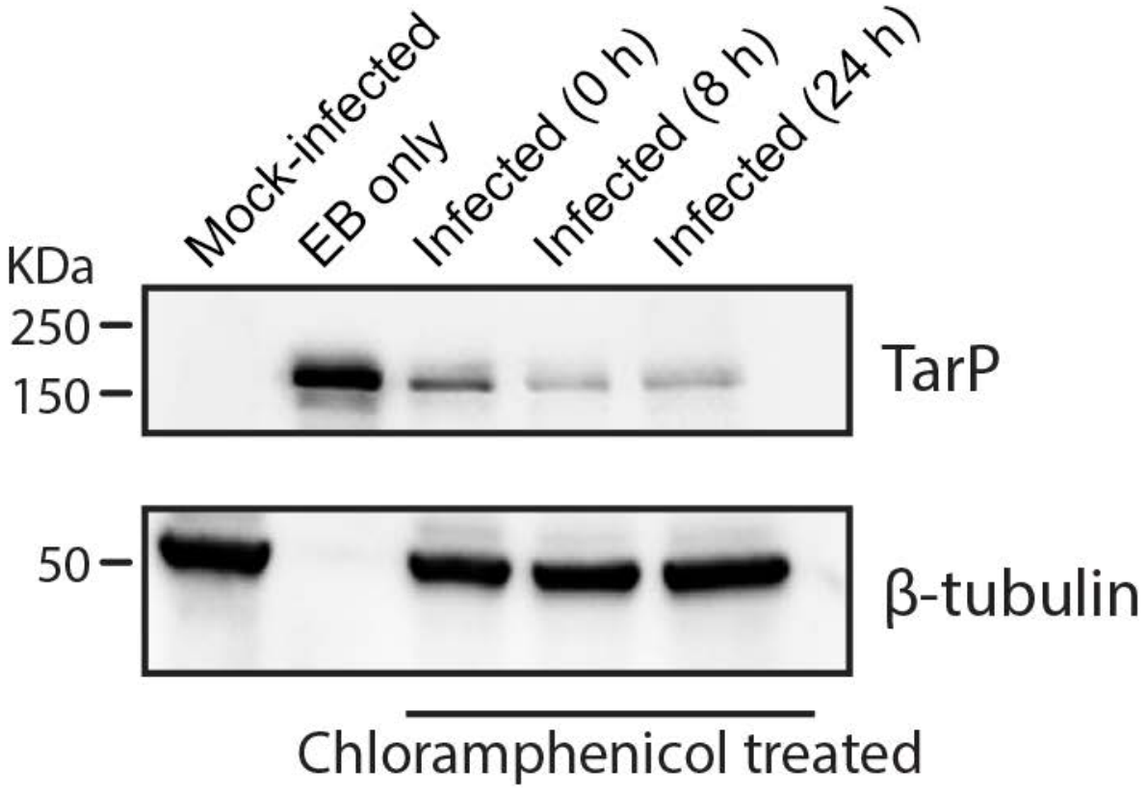
Mock-infected
EB only
Infected (0 h)
Infected (8 h)
Infected (24 h)
KDa
250
150
TarP
50
β-tubulin
Chloramphenicol treated

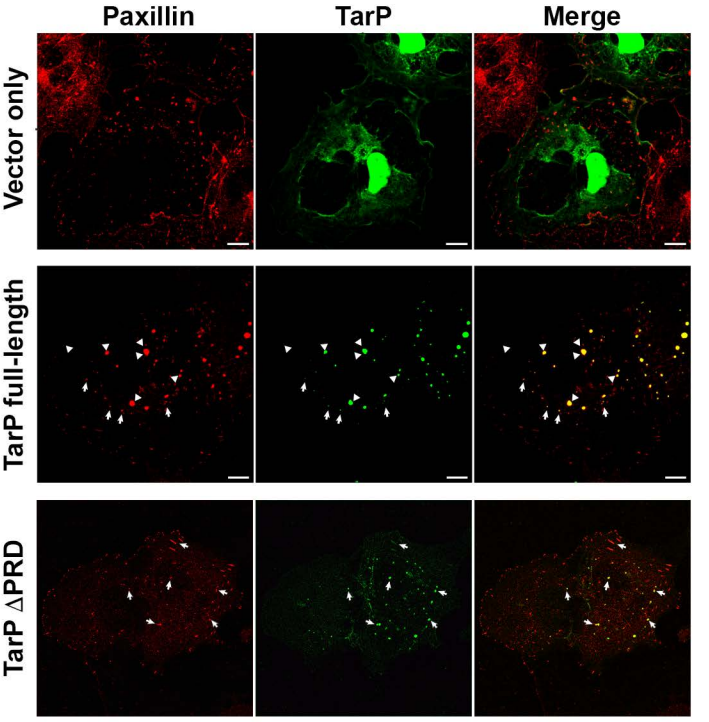

FIGURE S2

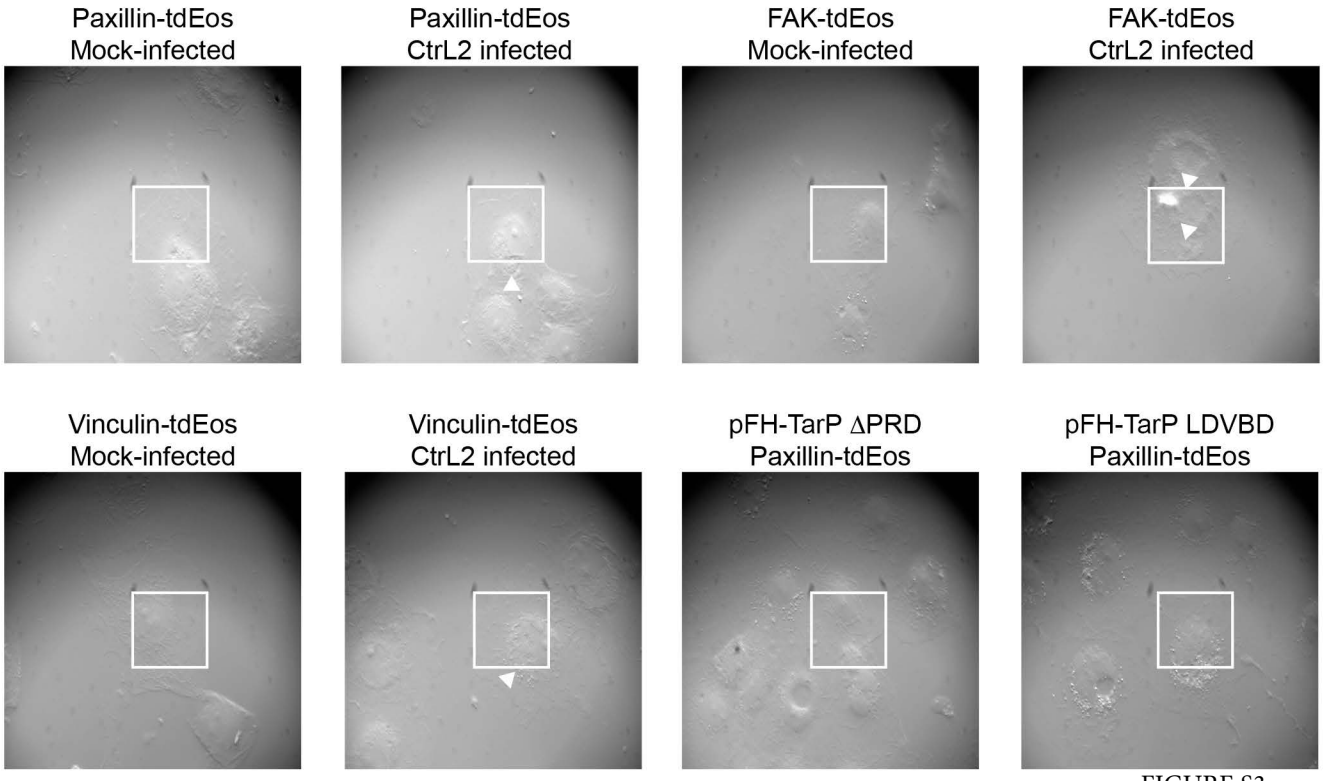
Paxillin-tdEos
Mock-infected
Paxillin-tdEos
CtrL2 infected
FAK-tdEos
Mock-infected
FAK-tdEos
CtrL2 infected
Vinculin-tdEos
Mock-infected
Vinculin-tdEos
CtrL2 infected
pFH-TarP ΔPRD
Paxillin-tdEos
pFH-TarP LDVBD
Paxillin-tdEos

FIGURE S3

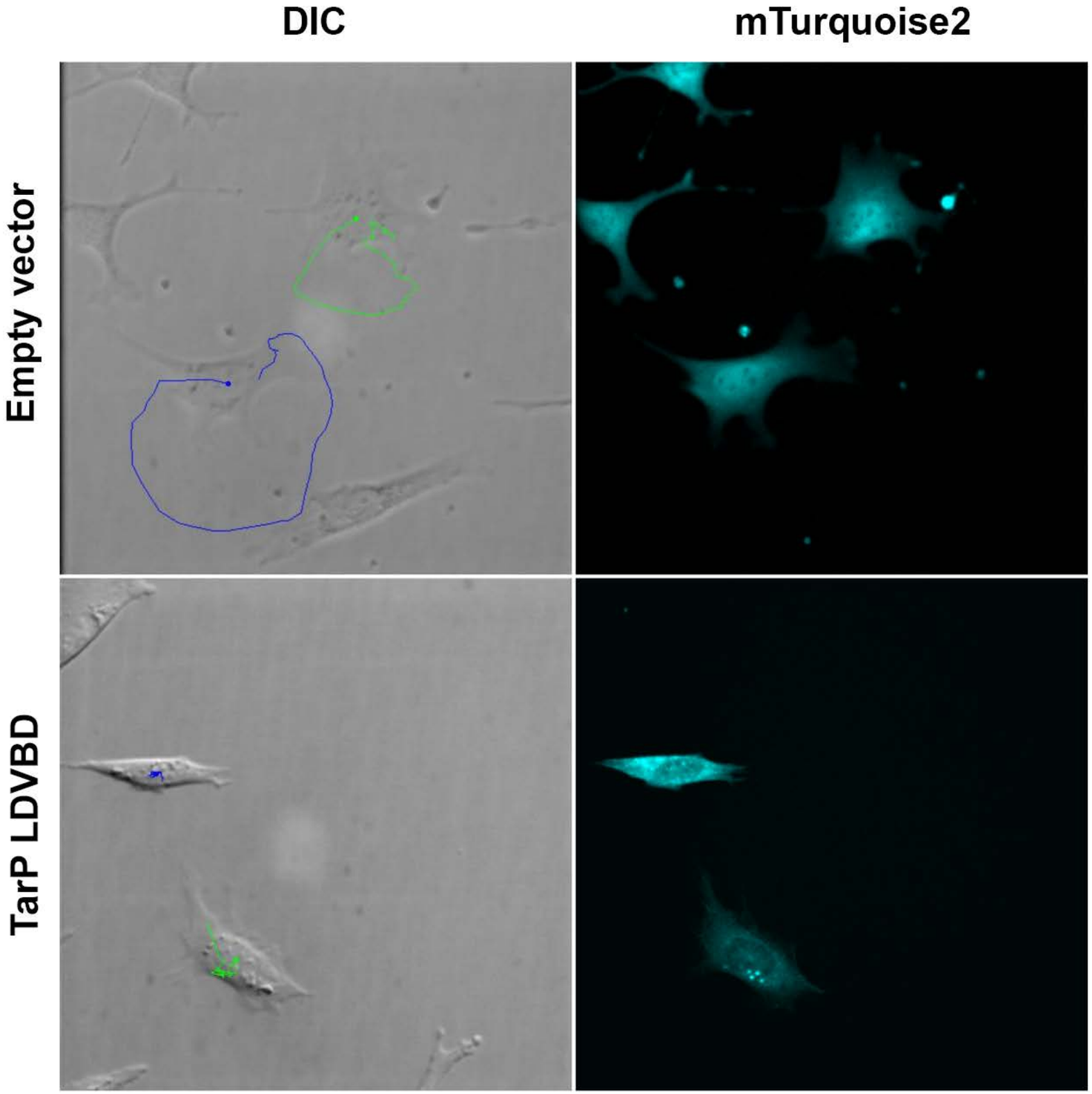

FIGURE S4